



Aberrant coiling signatures reveal the specialised reproductive strategy of the planktonic foraminifera *Neogloboquadrina pachyderma* under Central Arctic perennial sea ice

Tirza M. Weitkamp ^{a,b,*}, Clare Bird ^c, Kate F. Darling ^{c,d}, Allison Y. Hsiang ^{a,b}, Jemma Ramsay ^c, Flor Vermassen ^{a,b}, Helen K. Coxall ^{a,b}

^a Department of Geological Sciences, Stockholm University, Stockholm, Sweden

^b Bolin Centre for Climate Research, Stockholm University, Stockholm, Sweden

^c Biological and Environmental Sciences, University of Stirling, Stirling FK9 4LA, UK

^d School of Geosciences, University of Edinburgh, West Mains Road, Edinburgh EH9 3FE, UK

ARTICLE INFO

Keywords:
 Planktonic foraminifera
 Non-spinose
 Aberrant coiling
 Central Arctic Ocean
 Asexual reproduction
 Trimorphic

ABSTRACT

The perennially sea-ice covered Central Arctic Ocean (CAO) hosts a single planktonic foraminifera species, *Neogloboquadrina pachyderma*, a polar specialist that predominantly exhibits sinistral-coiling. Widely used as a palaeoceanographic proxy for polar conditions, it displays a range of morphologies, including an uncommon dextral form which resembles its subpolar relative, *Neogloboquadrina incompta*. The biological significance of dextral coiling in *N. pachyderma* remains unclear, complicating climate reconstructions and interpretations of its reproduction in the CAO. While culture studies link coiling direction to a biphasic life cycle involving an asexual stage producing both coiling types, supporting field data are lacking. This study analysed *N. pachyderma* collected from eight plankton net and four box core stations in the CAO beneath permanent sea ice. Morphometric and genetic analyses identified six *N. pachyderma* morphotypes concentrated in the upper 100 m, dominated by relatively small specimens (80–125 µm). Unusually high proportions of dextral coilers (up to 32 %) were observed in the water column, compared to ~6 % in the underlying sediment. Proloculus (first chamber) size-analysis and Gaussian Mixture Modelling revealed three proloculus-size means in the water column, suggesting the presence of an asexual clonal schizont generation alongside the typical sexual-aseexual cycle. These observations provide the first in situ evidence of schizont reproduction in natural *N. pachyderma* populations, a strategy that may facilitate rapid population growth and adaptability in the CAO. These results clarify the biological significance of coiling direction in *N. pachyderma*'s life cycle, and reduce the risk of misidentifying *N. incompta* in Arctic palaeoclimatic studies.

1. Introduction

The Central Arctic Ocean (CAO) represents one of the most extreme environments on Earth, for a large part characterised by permanent sea ice cover, limited energy availability, and highly seasonal pelagic primary production. Despite these challenges, it supports a functioning pelagic ecosystem including a single species of planktonic foraminifera: *Neogloboquadrina pachyderma* genetic Type 1a (Morard et al., 2024). This species has adapted remarkably to thrive even under thick sea ice and sea surface temperatures as low as -1.5°C in the CAO (Vermassen et al., 2025). Significantly, it produces a large proportion of total

sedimented biogenic carbonate in the Arctic (Huber et al., 2000; Anglada-Ortiz et al., 2021; Vermassen et al., 2025). *Neogloboquadrina pachyderma* is well known to palaeoceanographers through its long use in late Pleistocene climate studies. A defining morphological feature of the species is its strong preference for sinistral coiling (Darling et al., 2006). Historically, coiling direction was believed to be a phenotypically flexible feature under environmental control, with *N. pachyderma*'s coiling direction reversing (i.e. from sinistral to dextral) due to changes in water temperature over glacial-interglacial cycles (e.g. Ericson, 1959; Bandy, 1960; Thompson and Shackleton, 1980). Subsequent genetic studies have overturned this paradigm, revealing that preserved coiling

* Corresponding author at: Department of Geological Sciences, Stockholm University, Stockholm, Sweden.
 E-mail address: tirza.weitkamp@geo.su.se (T.M. Weitkamp).

shifts represent northward migrations/contractions of a genetically distinct dextral-coiling species, as it tracked its preferred habitat under changing climate states (Darling et al., 2006). The name *N. pachyderma* is now reserved for the sinistral forms typical of polar to subpolar conditions, while the dextral-coiling morphotype (formerly *N. pachyderma* [Type I (dex.)]) is assigned to *N. incompta*, which is limited to subpolar/transitional latitudes (Darling et al., 2006, 2023). Although coiling direction is strongly biased in both species—*N. pachyderma* is predominantly sinistral and *N. incompta* dextral—this coiling preference is not fixed. Genetic studies reveal that each species exhibits a low proportion (<3 %) of aberrantly coiled individuals, with even a small percentage (1–3 %) of dextral coiling *N. pachyderma* found in polar planktonic assemblages (e.g. Pflaumann et al., 1996; Bauch et al., 2003; Darling et al., 2004; Darling et al., 2023).

Recent plankton surveys confirm that *N. pachyderma* remains the only planktonic foraminiferal species inhabiting the polar ocean beneath the perennial sea ice of the Central Arctic: in summer 2021, it comprised 100 % of water column populations, with the exception of single site within the ice pack located near the sea-ice edge on the Yermak Plateau (Station SO21–58-16), where a very limited number of *Turborotalita quinqueloba* specimens were found (Vermassen et al., 2025). *Neogloboquadrina pachyderma* has a pronounced morphological variability (e.g. Vilks, 1973, 1975), with five sinistrally coiling morphotypes (Nps-1 through Nps-5) recognised based on wall texture, coiling, chamber shape and chamber number (Eynaud et al., 2009; Eynaud, 2011; El Bani Altuna et al., 2018). A dextral coiling morphotype, which genetic analyses confirm to be aberrant coiling *N. pachyderma* (Bauch et al., 2003; Darling et al., 2006), is also routinely present in *N. pachyderma* populations in low numbers. In this study, the dextral coiling form is referred to as 'Npd'. To date, the aberrant coilers have been found to represent a predictable ca. 3 % of populations (Pflaumann et al., 1996; Bauch et al., 2003; Darling et al., 2023). According to this current paradigm, any proportion of dextral coilers above this threshold should be interpreted as evidence of an incursion of *N. incompta* and by inference, evidence of climatic and oceanic warming (Bauch et al., 2003; Darling et al., 2006). However, it is unknown how robust this 3 % threshold is in the under sampled Central Arctic Ocean.

The biological significance of *N. pachyderma* morphotypes remains poorly understood (El Bani Altuna et al., 2018; Prabhakar et al., 2024). Culture and morphology studies hypothesise that Nps-5 (a lightly calcified 4 to 5-chambered form) and the dextral coilers may represent stages in a multi-generational life cycle that includes agamonts (diploid) produced by sexual reproduction and immature gamonts (haploid) produced through asexual reproduction (Davis et al., 2020; Darling et al., 2023; Meilland et al., 2022, 2024). An additional facultative third generation, where successive asexual generations (diploid schizonts) are cloned by the agamont, has been observed in *N. pachyderma* cultures (Meilland et al., 2024). However, supporting field evidence is missing. Insights from benthic foraminifera, more readily studied in their natural environments, offer important clues about reproductive strategies. Benthic foraminifera are known to have complex life cycles that often include two distinct reproductive forms or morphotypes within the same species (e.g. Dettmering et al., 1998; Goldstein, 2002). Such dimorphs are typically linked to sexual and asexual stages and may be distinguished by differences in test and proloculus size (i.e. first chamber that forms around a haploid or diploid embryo) (Darling et al., 2023).

While planktonic foraminifera were long assumed to reproduce only sexually (Hemleben et al., 1989), recent culture studies have revealed that some non-spinose planktonic foraminifera species, such as *N. pachyderma* and *Globigerinita uvula*, are also capable of asexual reproduction (Davis et al., 2020; Takagi et al., 2020; Meilland et al., 2022, 2024), thereby challenging earlier assumptions. Asexual reproduction, however, currently remains unknown in the majority of other planktonic foraminifera species. In addition, patterns of low-level (<3 %) aberrant coiling similar to those observed in *N. pachyderma* are documented in other non-spinose macroperforate species (Brummer

et al., 1987). Moreover, culture reproductive events are inevitably opportunistic (Davis et al., 2020; Meilland et al., 2022, 2024) and cannot fully emulate the natural populations of the water column. The different reproductive modes and their proportionality in a natural water column population sample have never been observed in the wild. Since no universal rules appear to link specific proloculus sizes (e.g. small or large) with a specific sexual or asexual stage (Darling et al., 2023), each species must be assessed on its own. Given that modern planktonic foraminifera evolved from various benthic ancestors (i.e. they are polyphyletic; Morard et al., 2024), we must remain open to new life cycle models based on emerging data.

Here, we present the first 'wild' in situ evidence exploring the link between test morphology, coiling direction and asexual reproduction in *N. pachyderma*. Measurements were made on a dataset of ca. 15,000 specimens collected from water-column and sediment assemblages across eight plankton-net and four box core stations in the Central Arctic Ocean during summer 2021 (Fig. 1). Genotyping was conducted to verify if *N. pachyderma* Type 1a was the only genotype present in the assemblages sampled. Using a combination of both automated and manual imaging combined with morphometric approaches, we recorded coiling direction together with measurements of test size, shape, and proloculus size to address the following hypotheses and questions: Are the six *N. pachyderma* morphotypes, found previously in sediments, present in Arctic water column populations? If so, what does their vertical distribution tell us about their ecological or ontogenetic significance? Is the 3 % maximum aberrant coiling threshold maintained in Central Arctic plankton populations? Does the multi-stage life cycle associated with differences in proloculus size include the presence of a schizont generation? As the Central Arctic Ocean hosts only *N. pachyderma* Type 1a, it is uniquely suited to answering these questions. With no other species to complicate the picture (Darling et al., 2023; Morard et al., 2024), the CAO is in effect a natural *N. pachyderma* laboratory. Unravelling the ecological traits of *N. pachyderma*, including the strategic role of asexual reproduction in its life cycle, is vital for understanding the success and resilience of this unique polar species.

2. Methods

2.1. Planktonic foraminifera sampling

The Synoptic Arctic Survey expedition with *I/B Oden* (SAS-Oden21) was carried out from August 2nd to September 11th 2021 (Snoeijns-Leijonmalm and the SAS-Oden Scientific Party, 2022) (Fig. 1; Supplementary Table 1). Plankton samples were obtained from eight stations (hereafter referenced by their corresponding station numbers in Fig. 1) using a multiple open-closing (lever-operated) plankton sampler net (multinet; Multi Plankton Sampler MultiNet® Type Midi by Hydro-Bios) with a mesh size of 55 µm. Five samples per cast were collected from five depth intervals: 0–50 m, 50–100 m, 100–200 m, 200–500 m and 500–1000 m. The upwards towing speed was 0.5 m/s. After deployment, the multinet was sprayed down with seawater to concentrate remaining plankton material into the collection cups. The depth-specific plankton samples were poured into storage containers with additional filtered seawater (0.2 µm) from the same location and depth in preparation for examination. Samples were processed immediately after they were collected, starting with the shallowest net since this contained the most material. All picking was carried out in a cold lab at ambient temperature (~2–8 °C). Aliquots from the main storage container were pipetted onto a shallow glass dish from the plankton concentrates in the collection cups and examined shipboard under a Zeiss Stemi 508 light microscope using reflected (incident) light from above and on a black background. Planktonic foraminifera were identified among the other zoo- and phytoplankton.

For genotyping, 30–60 specimens were collected from Stations 1, 2, 4 and 8. Using a fine brush (size 3/0), specimens were cleaned in 0.2 µm filtered seawater taken from the same location and depth. Specimens

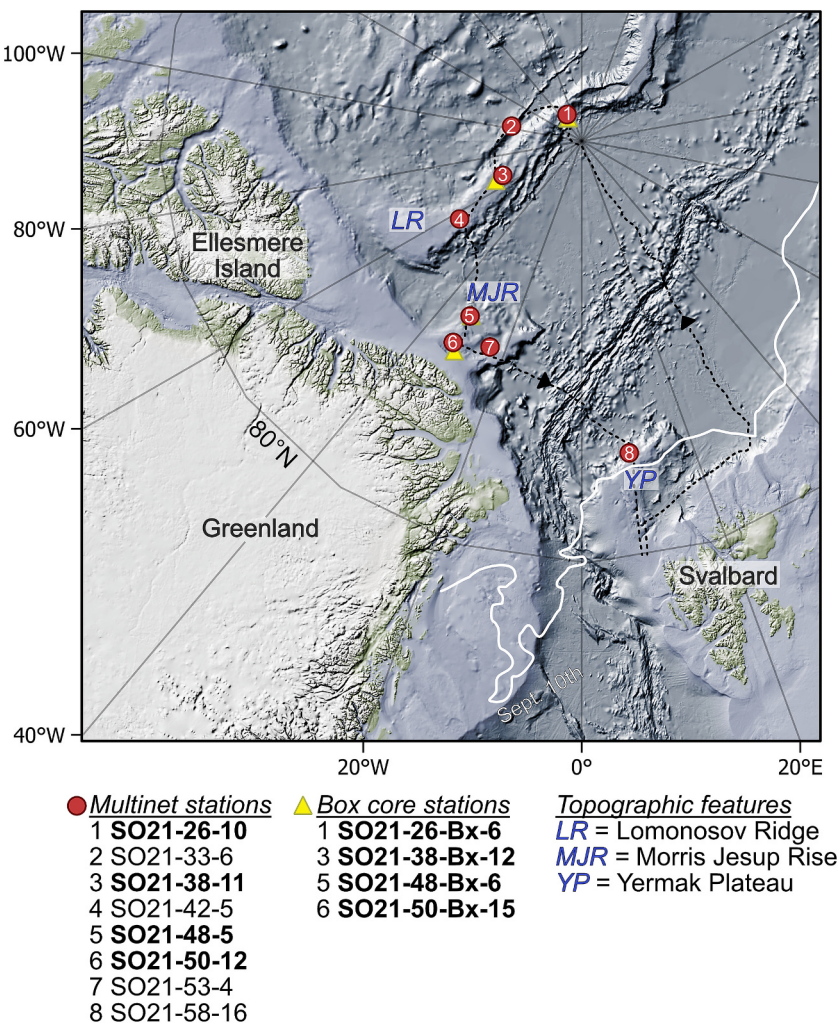


Fig. 1. Bathymetric map of the Arctic Ocean (Jakobsson et al., 2020) showing the SAS ODEN 2021 Expedition sampling stations relevant to this study. Multinet stations are indicated by a red circle, box core stations with a yellow triangle. Paired plankton-sediment stations are indicated by bold type. Sample stations are numbered according to the order of sampling between 19/08/2021 and date 11/09/2021 (Supplementary Table 1), the ship track direction is indicated with the black line. The sea ice extent minimum is indicated with the white line (September 10th 2021) (data US NIC). (For interpretation of the references to colour in this figure legend, the reader is referred to the web version of this article.)

were then momentarily placed on a micropaleontological slide to remove the seawater before being transferred individually into a 0.5 mL screwcap microfuge tube containing 100 μ L of RNAlater® (Ambion™). Samples were stored at ambient temperature for four hours before freezing at -20°C . The remaining individuals were then picked onto microfossil slides using a fine brush. Samples that could not be picked shipboard due to time limitations were preserved in an ethanol solution and picked post cruise (December 2021 – May 2022) at the Department of Geological Sciences, Stockholm University. Planktonic foraminifera were then placed on microscope slides in their umbilical position, identified to species and morphotype level, and counted to record the abundance of planktonic foraminifera per depth-ordered net sample. Station information can be found in Supplementary Table 1.

Box coring (50x50x60 cm) was done at six stations (Fig. 1) during the SAS expedition, corresponding to the multinet stations (Snoeijs-Leijonmalm and the SAS-Oden Scientific Party, 2022). Core top sediment samples were taken from the upper 0–1 cm of each box core. Sediment samples were washed over a $>63\text{ }\mu\text{m}$ sieve and oven dried at ca. 50°C overnight. The number of planktonic foraminifera per sample in the $>63\text{ }\mu\text{m}$ fraction was recorded by making counts on split samples from the dried $>63\text{ }\mu\text{m}$ fraction. The samples were split using a microsplitter to produce subsamples containing approximately 300 specimens. These

subsamples were then examined under the light microscope, where all specimens were identified and counted. These counts were based on the standard method of identifying about 300 individual per sample, providing a representative estimate of the assemblage composition. For the box core stations 1, 3, 5, and 6, all sedimented planktonic foraminifera were picked from the split and placed on micropaleontological slides for imaging and morphometric analysis.

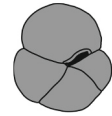
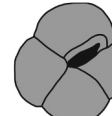
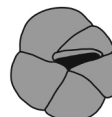
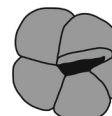
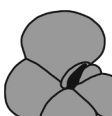
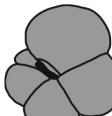
Our sampling in the perennially sea-ice-covered Central Arctic Ocean focused on a region of the ocean where we were confident that only a single genotype of our target species *N. pachyderma* Type Ia resides (Darling et al., 2023). This was further confirmed using targeted genotyping (see Section 2.5).

2.2. *Neogloboquadrina pachyderma* morphotypes

Planktonic foraminifera were identified to species level by traditional human-based microscope observations, following the taxonomic framework of Schiebel et al. (2017), with *N. pachyderma* morphotype-level definitions of Eynaud et al. (2009), Eynaud (2011), and El Bani Altuna et al. (2018). Minor elaborations of the *N. pachyderma* morphotype concepts made in this study are included in Table 1. Aside from a few specimens of *Turborotalita quinqueloba* at Station 88, all specimens

Table 1

Morphological descriptions and drawings of the six *N. pachyderma* morphotypes, derived from water column and sediment specimens. Classification follows Eynaud et al. (2009), Eynaud (2011) and El Bani Altuna et al. (2018). Morphometric data sourced from Supplementary Tables 7 and 8.

Morphotype	Description
Nps-1	<p>Encrusted small sized individuals with 4 chambers in the final whorl. Test shape is compact and rhombic, height is longer than width. Sutures on spiral and umbilical side obscured by high level of encrustation. The aperture is small and extra-umbilical and often obscured by the final chamber. A well-defined lip can be present.</p> <p>Plate 1: Figs. 1-3 Plate 2: Figs. 1-3</p> <p>Average aspect ratio: 1.11 (water column, 1.13 (sediment) Average major axis: 185.8 μm (water column), 165.2 μm (sediment) Average minor axis: 158.9 μm (water column), 139 μm (sediment)</p> 
Nps-2	<p>Quadrat specimens with four (sub)equal globular chambers, a large aperture, and prominent apertural lip. The sutures on the umbilical side form a cross.</p> <p>Plate 1: Figs. 4-6 Plate 2: Figs. 4-6</p> <p>Average aspect ratio: 1.06 (water column and sediment) Average major axis: 215.3 μm (water column), 206.9 μm (sediment) Average minor axis: 193.6 μm (water column), 185.8 μm (sediment)</p> 
Nps-3	<p>Elongated specimens with a large aperture and 4-4.5 subglobular chambers. A lip can be present. The majority of specimens have a kummerform final chamber.</p> <p>Plate 1: Figs. 7-9 Plate 2: Figs. 7-9</p> <p>Average aspect ratio: 1.11 (water column & sediment) Average major axis: 215.2 μm (water column), 227.2 μm (sediment) Average minor axis: 183 μm (water column), 192.2 μm (sediment)</p> 
Nps-4	<p>Largest morphotype, with a globular to quadrat outline. Specimens have 4-4.5 globular chambers in the final whorl. The aperture is deep and large with a well-defined lip.</p> <p>Plate 1: Figs. 10, 11 Plate 2: Figs. 10-12</p> <p>Average aspect ratio: 1.09 (water column), 1.10 (sediment) Average major axis: 250.2 μm (water column), 265.5 μm (sediment) Average minor axis: 218.5 μm (water column), 232.2 μm (sediment)</p> 
Nps-5	<p>This morphotype consists of immature and mature individuals that have in common a thin, translucent, globular test.</p> <p>Mature specimens ($>125 \mu\text{m}$) have 4 globular chambers in the final whorl. The initial whorl on the spiral side is visible in light microscope and SEM images. Sutures on spiral and umbilical side are deep. The aperture is large and open, umbilical to extra-umbilical. A well-developed lip can be present. Wall texture is a combination of protuberances. The euhedral calcite crystals on Nps-1 through Nps-4 are absent in Nps-5.</p> <p>Immature specimens ($<125 \mu\text{m}$) have 4-5 chambers in the final whorl. The aperture is a slit with a well-developed lip. On the spiral side the pores are located in the sutures of the initial whorl. After the 6th chamber (initial whorl) the pores move toward the inner chamber region (Plate 3, Fig. 14). Wall texture varies from smooth to having a combination of protuberances. The pore sizes in the initial whorl are $>1 \mu\text{m}$, consistent with a macroporiferous wall structure.</p> <p>Plate 1: Figs. 12-14 Plate 2: Figs. 13-15 Immature specimens: Plate 3</p> <p>Average aspect ratio: 1.17 (water column), 1.19 (sediment) Average major axis: 126.2 μm (water column), 132.4 μm (sediment) Average minor axis: 97.1 μm (water column), 102.8 μm (sediment)</p> 
Npd	<p>All right coiling specimens, including the dextral coiling equivalent of Nps-1 through Nps-5 and immature individuals (Plate 3).</p> <p>Plate 1: Figs. 15-19 Plate 2: Figs. 16-20</p> <p>Average aspect ratio: 1.15 (water column), 1.13 (sediment) Average major axis: 129.6 μm (water column), 161.8 μm (sediment) Average minor axis: 104.8 μm (water column), 132.1 μm (sediment)</p> 

were identified as *N. pachyderma*, both in the net and sediment samples. All five sinistrally coiled morphotypes (Nps-1 through Nps-5) were recognised, as well as the dextrally aberrant coiling morphotype Npd. We note that the Nps-5 morphotype concept used in this study comprises small to large, relatively smooth-walled (optically reflective), thin-shelled specimens, whereas Nps-1 through Nps-4 have rugose, thickened tests. Morphological variability was also observed within the dextral Npd morphotype category. They exhibited a similar scale of variability represented by the Nps-1 to Nps-5 categorisation (Plate 1, Figs. 15–19 and Plate 2, Figs. 16–20), but were all grouped under the single Npd category in this study.

Scanning electron microscope (SEM) imaging was carried out on a subset (ca. 400 specimens) of well-preserved specimens to document the morphotypes and taxonomic concepts. Imaging was carried out using a JSM-7000 F SEM, housed at the Department of Materials and Environmental Chemistry, Stockholm University (accelerating voltage = 10 kV, working distance = 10 mm). Specimens were mounted on sticky carbon disks and gold coated (5 nm thick) before analysis (2 × 60 s, applied current of 20 mA).

2.3. High throughput imaging and morphometric analyses

For morphometric analysis, an automated imaging and measurement approach was used. All plankton tow ($n = 15,733$) and sediment ($n = 1908$) specimens were manually placed in the umbilical position to ensure consistent identification of dextral and sinistral morphologies. Specimens were grouped into the following categories on separate microscope slides: Nps-1 through Nps-5 and Npd (Plates 1, 2; Table 1). All specimens were imaged at 200 \times using a Keyence VHX-7000 digital microscope fitted with an automatic XYZ stage, producing focus-stacked full slide images. Individuals were segmented from the collected images using the ‘segment’ module of AutoMorph, a computational tool designed to quantify and analyse shape variation in biological and fossil specimens (Hsiang et al., 2018). This approach automatically separates objects from their imaged background using traditional image processing methods. Threshold values ranged from 0.38 to 0.45 and size ranged from 15 to 500 μm depending on specific image characteristics. Optimal parameter values were chosen to maximise the number of individuals correctly segmented. Pixel size varied between 0.735 and 2.884 $\mu\text{m}/\text{pixel}$ and was used to scale the x- and y-axes based on output from the Keyence VHX-7000 microscope. After the optimal parameter values were identified via manual testing, the images were processed under ‘Final’ mode in AutoMorph using the batch-processing mode to obtain individual cropped images of each specimen. A total of 14,989 water column and 11,882 sediment specimens were segmented (Tables S2–S4). Incorrectly identified non-foraminifera material, e.g. images of the slide background texture, were removed manually in post-processing. An example of the workflow is shown in Fig. S1.

All specimen images were grouped into their appropriate sample station and water column/sediment depth interval and processed using the ‘run2dmorph’ module of AutoMorph. This module detects the outlines of individuals and then automatically extracts morphometric measurements such as major/minor axis length, perimeter length, area, etc. Default values were used for all input parameters to ‘run2dmorph’, except for disk size opening and contrast adjustment. Disk size opening values were set to 25 and contrast adjustment values varied between 2 and 3.

From the water column, 14,989 individuals were segmented using AutoMorph, of which 14,730 were successfully measured. In the sediment samples, 1882 individuals were segmented, with 1791 successfully measured. Imperfect outlines (i.e., those that did not fully capture the individual or included background noise (Supplementary Fig. 3), were manually removed during post-processing. This resulted in final morphometric data for 12,896 water column and 11,713 sediment specimens. The area, major and minor axis, and XY ratio were used to quantitatively characterise each morphotype (Supplementary Fig. 2).

Major axis length (Supplementary Table 5) was used to separate the morphotypes into size classes, whereas the area vs XY ratio was used to characterise the morphotypes (Supplementary Table 8).

The vertical distribution pattern of each morphotype per station is expressed as the proportion of raw standing stock counts (Supplementary Tables 2–4). These proportions are based on the dataset before morphometric cleaning (i.e., 14,370 water column and 11,791 sediment specimens), as approximately 14 % of the water column specimens were discarded during data cleaning for morphometric analysis due to e.g. irregular outlines. This study mainly focuses on the relative abundance of morphotypes, and therefore, the normalised data on the vertical distribution were not utilised. The normalised abundances on the vertical distribution of planktonic foraminifera from the SAS-Oden 2021 expedition can be found in Vermassen et al. (2025).

Previous studies have shown that test size within a species corresponds to growth and ontogenetic stage (Brummer et al., 1987; Duan et al., 2021). All morphotypes were classified into three size classes to distinguish life stages based on culture and sediment observations of *N. pachyderma*: juveniles (<80 μm ; Davis et al., 2020), neanic (80–125 μm , >80 μm ; Davis et al., 2020), and mature (>125 μm ; El Bani Altuna et al., 2018) (Supplementary Fig. 4). The >125 μm and > 150 μm size fractions are frequently used in palaeoceanographic studies. Use of the >125 μm size fraction also allows comparison to the results of El Bani Altuna et al. (2018) from Canadian Arctic Archipelago core tops. The >150 μm size fraction (large mature) was specifically included for comparison with the results of Prabhakar et al. (2024), who focused on this larger size fraction in their sediment studies from Siberian and Central Arctic core tops (Tables S9, S10). Morphotypes Nps-5 and Npd were further classified by water column depth interval and size class to assess the depth-related habitat distribution in relation to size (Supplementary Tables 11 and 12).

2.4. Testing for dimorphism: proloculus size and Gaussian mixture modelling

To gain insights into the potential multiple life stages, we measured the proloculus size on 231 randomly picked translucent sinistral and dextral *N. pachyderma* (ca. 14 % of the assemblage) from Station 4 (0–50 m water depth plankton net), where one of the highest abundances of Npd was observed (Supplementary Tables 5 and 6). The proloculus is only visible in SEM images in these small, thin-walled juvenile specimens; in more mature specimens with heavily calcified tests, the proloculus is obscured by adult whorls and successive calcite layers. SEM imaging was performed on the spiral side of each specimen and the external proloculus size was measured manually using ImageJ (Schneider et al., 2012).

To explore the distribution of proloculus size (Supplementary Table 13) in the dataset, Gaussian Mixture Models (GMMs) were used employing Expectation Maximization (EM) algorithms to investigate the possible underlying univariate normal distributions that give rise to the observed data patterns. GMMs allow us to model complex multimodal distributions as a mixture of individual Gaussian distributions, whereby each Gaussian distribution represents a cluster in the underlying data with associated interpretable parameters. The analyses were carried out using RStudio v.2023.06.0 + 421 (RStudio Team, 2020) and run separately on the sinistral and dextral datasets. Model-based GMM clustering was run using the R package Rmixmod v.2.1.10 (Lebret et al., 2015), which previous work suggests estimates mixture parameters with smaller bias than other implementations of the EM algorithm in R (Chassagnol et al., 2023).

The *mixmodCluster* function in Rmixmod was used to fit GMMs to our data. To determine the best-fit number of components (i.e. Gaussian distributions that comprise each finite mixture) for each dataset, we conducted model testing using a range of 1 to 5 components to explore whether the data distribution is best explained by a single homogenous cluster or by multiple independent clusters. The latter would be

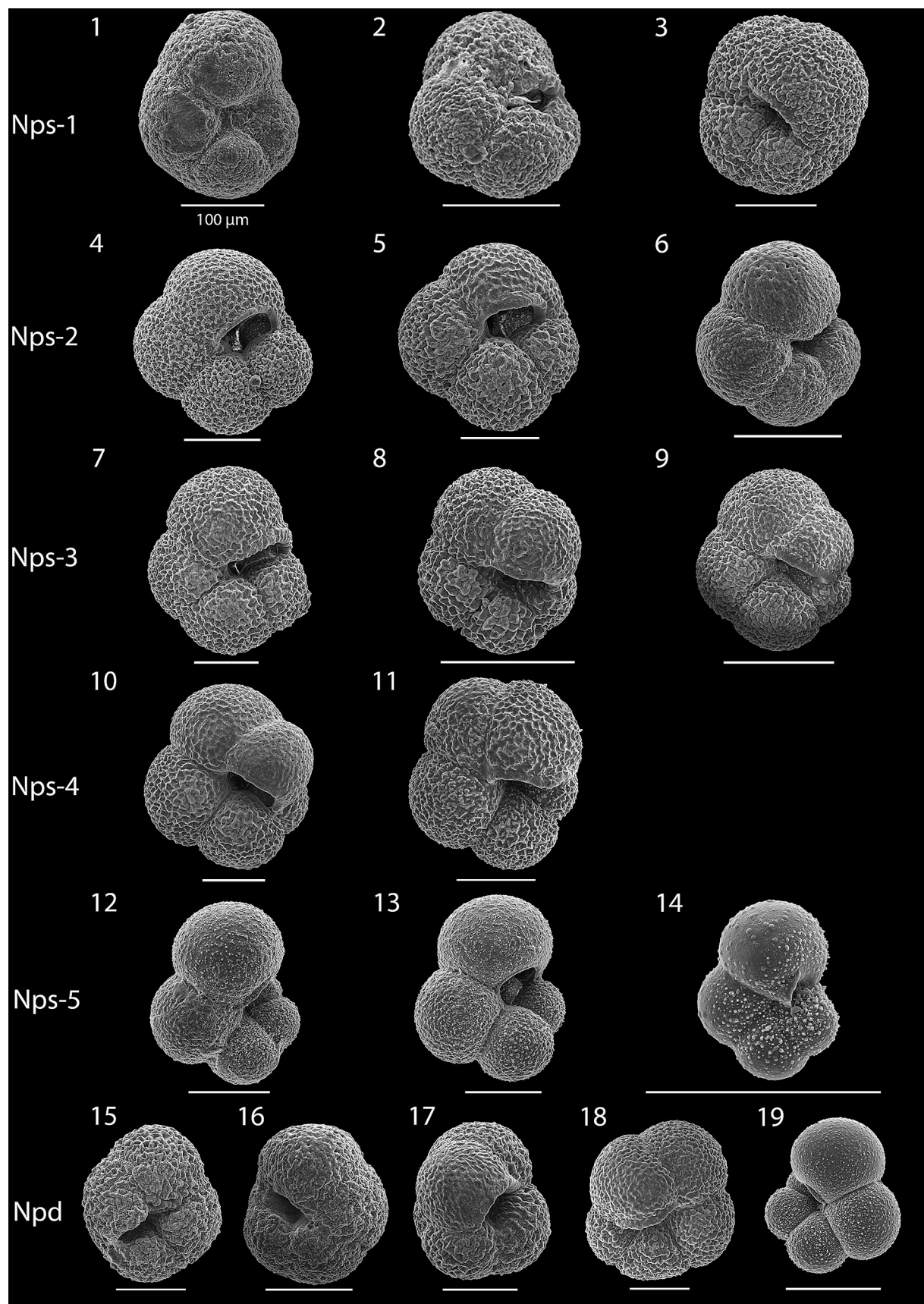


Plate 1. Water column *N. pachyderma* morphotypes. 1–3 Nps-1 (1, 2: SO21–58-16, 50–100 m; 3: SO21–58-16, 100–200 m), 4–6 Nps-2 (4: SO21–58-16, 100–200 m; 5, 6: SO21–53-4, 500–975 m), 7–9 Nps-3 (7: SO21–58-16, 100–200 m; 8: SO21–42-5, 50–100 m; 9: SO21–53-4, 500–975 m), 10–11 Nps-4 (10: SO21–50-12, 0–50 m; 11: SO21–42-5, 50–100 m), 12–14 Nps-5 (SO21–50-12, 0–50 m), 15–19 Npd (15–17: SO21–48-5, 100–200 m; 18: SO21–53-4, 500–975 m; 19: SO21–58-16, 100–200 m). All scalebars are 100 µm, unless otherwise indicated. Figs. 3, 5, 7, 10, 12 and 13 are re-imaged from [Vermassen et al., 2025](#).

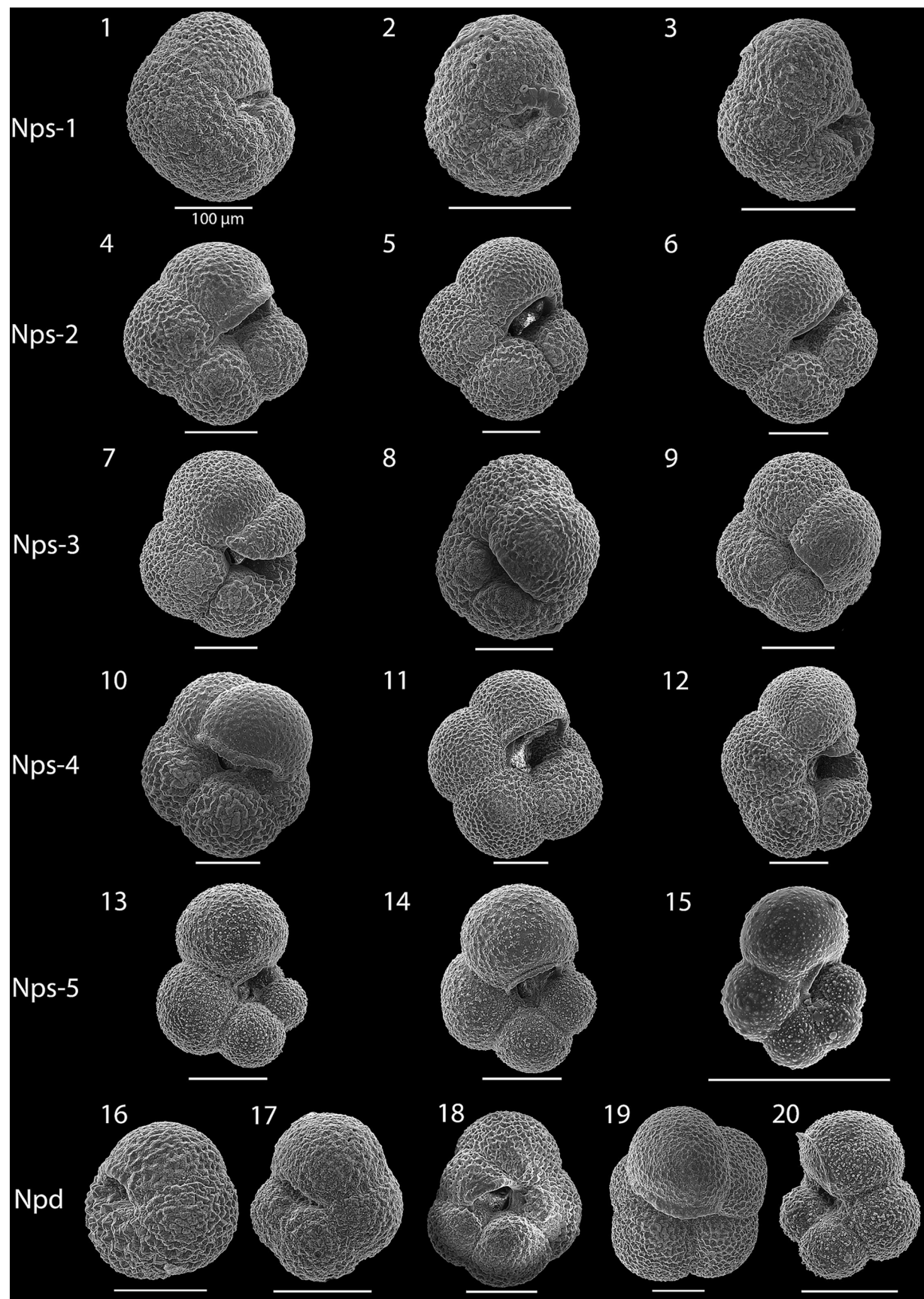


Plate 2. Surface sediment *N. pachyderma* morphotypes. 1–3 Nps-1 (1: 38-Bx-12, 0–1 cm; 2, 3: 48-Bx-6, 0–1 cm), 4–6 Nps-2 (4: 50-Bx-15, 0–1 cm; 5: 38-Bx-12, 0–1 cm; 6: 48-Bx-6, 0–1 cm), 7–9 Nps-3 (7–9: 48-Bx-6, 0–1 cm), 10–12 Nps-4 (10: 48-Bx-6, 0–1 cm; 11–12: 38-Bx-12, 0–1 cm), 13–15 Nps-5 (13, 14: 50-Bx-15, 0–1 cm; 15: 48-Bx-6, 0–1 cm), 16–20 Npd (16, 18, 20: 38-Bx-12, 0–1 cm; 17, 19: 48-Bx-6, 0–1 cm). All scalebars are 100 μ m, unless otherwise indicated.

expected if varying reproductive strategies resulted in distinct populations with discriminable morphological characteristics. All available criteria for model selection were applied (i.e., Bayesian information criterion [BIC], integrated classification likelihood [ICL], and normalised entropy criterion [NEC]). All other parameters were set to default values (algorithm = EM, number of iterations = 200, epsilon = 0.001). Because the model fitting process is stochastic, we ran 50 replicates of each model testing analysis. Inspection of the results shows that all successful analyses converged upon the same optimal number of clusters and likelihood values (within an absolute difference of 1.0×10^{-4}). Some replicates failed due to numerical errors that arise from incompatible starting values; in this case, four of the replicates for the dextral dataset analyses failed. The component parameters (means [μ], standard deviations [σ]), and weights [λ]) were then averaged over all iterations.

2.5. Genotyping of individual *N. pachyderma*

For genotyping, a total of 40 cloned sequences (Supplementary Table 14) were obtained from specimens ($n = 18$) collected at Stations 2 and 8, which represents the broadest distance across the cruise track. Station 2 represents an area of high relative abundance of dextral coiling in the *N. pachyderma* population under the perennial sea ice (Fig. 3). Station 8 represents a region that has only a marginally elevated percentage of dextral coiling specimens compared to the recognised 3 %, but also has a broader diversity of foraminiferal species present, since *T. quinqueloba* was morphologically identified at this site. Individual samples from additional stations where there was a high percentage of dextral coiling, (5, 6 and 7) could not be picked due to the rapid succession of net deployments. These samples were instead immediately preserved in EtOH for onshore picking.

DNA extractions were carried out on samples stored in RNALater® post cruise at the University of Stirling. First, cells were washed in sterile salt-adjusted phosphate buffered saline (PBS with 24.62 g/L NaCl added) to remove the RNALater® and transferred to 40 μ L DOC buffer for DNA extraction (Holzmann and Pawlowski, 1996). PCR amplifications were then carried out according to Bird et al. (Bird et al., 2024, in review). Cloning was carried out directly with PCR products using the TOPO-TA cloning kit according to the manufacturer's protocol (Invitrogen). Sequencing was performed using a BigDye Terminator v3.1 Cycle Sequencing kit (Applied Biosystems), and sequencing reactions were sent to Source Bioscience (Cambridge, UK) for Sanger sequencing.

3. Results

3.1. *Neogloboquadrina pachyderma* morphotype distribution in the CAO

Our datasets document distributions of morphotypes in the water column and identify significant differences between the netted and sedimented assemblages (Fig. 2). Average sea-ice thickness at our stations was $1.77 \text{ m} \pm 48 \text{ cm}$, as measured by ice core length (Snoeijns-Leijonmalm and the SAS-Oden Scientific Party, 2022). However, this is likely an upper estimate due to site selection bias favouring thicker sea ice for practical considerations (e.g. stability of ship parking) and safety. We confirm that *N. pachyderma* was the only planktonic foraminifera species found in both the Central Arctic water column and underlying sediments samples using both test morphology and DNA genotyping, of which the latter was performed on individuals from Stations 2 and 8 (Fig. 1, Supplementary Table 14, NCBI accession numbers PV277659-PV277698). The only exception was the Yermak Plateau (Station 8; Fig. 1), the most southerly and peripheral Arctic station close to Atlantic Water Influence, where a low percentage (26 individuals ($>55 \mu\text{m}$ size fraction), ca. 1 % of the assemblage; 0–1000 m water depth) of *Turborotalita quinqueloba* was found. These individuals were not included in the morphometric analyses.

A total of 14,370 *N. pachyderma* specimens from the water column were classified into the six morphotypes (Nps-1 through Nps-5 and Npd;

Table 1) using AutoMorph segmentation (Plate 1). Sinistral-coiling morphotypes (Nps-1 to Nps-5) comprised 11,118 specimens, while dextral-coilers (Npd) accounted for 3252 specimens. The highest total standing stock of *N. pachyderma* was recorded at Station 5, with 3135 specimens (Fig. 2E). At all other stations, *N. pachyderma* was most abundant in the upper 100 m of the water column (Fig. 2, Supplementary Table 6), except at Station 8, where its highest abundance occurred between 50 and 500 m, though with lower overall numbers of Npd compared to the other stations. Nps-5 was the most abundant morphotype in the water column (69.3 % on average), usually down to 1000 m water depth. Its total abundance decreased as the proportion of other morphotypes (particularly Nps-1-4) increased with depth, with highest numbers found between 50 and 200 m (Fig. 2, Supplementary Tables 5 and 6). Nps-4 was the least common morphotype (ca. 0.4 %, Supplementary Tables 5–7). Most surprising was the high abundance of Npd, which made up 21.3 % of the water column (0–1000 m) population on average (range 8.8–32.3 %; Supplementary Table 6).

The highest relative abundances of Npd were found at Stations 5 and 6 (32.3 % and 28.4 %, respectively; Supplementary Table 6). These stations are located at similar latitudes and were sampled only a few days after each other (Fig. 3 Supplementary Tables 1 and 8). We do not consider these right coiling forms to be *N. incompta* because this species is restricted to the warmer subpolar and transitional waters (e.g. Darling et al., 2006, 2023) and would not be able to live in the CAO where sea surface temperatures are as low as -1.5°C (Vermassen et al., 2025). Additionally, *N. incompta* was not identified in our genetic analysis. A linear regression was performed to assess the relationship between the relative abundance of Npd and the relative timing/location of the sampling in terms of time of year/season and ship track. When all eight stations are included, the regression showed a non-significant relationship ($R^2 = 0.03, p = 0.683$; Fig. 3, blue line). However, excluding Station 8 positioned close to the sea-ice edge at the periphery of the CAO (Yermak Plateau), the central Arctic perennial sea ice area showed a statistically significant relationship ($R^2 = 0.801, p = 0.00649$; Fig. 3, green line) in the CAO.

A total of 1791 *N. pachyderma* specimens from surface sediment samples were also classified into the six morphotypes (Plate 2), with 1689 being sinistral (Nps-1 through Nps-5) and 102 being dextral (Npd) (Supplementary Table 9). Although Nps-5 was a dominant component of the water column assemblage, it was less dominant in seafloor sediments (on average 39.6 %, Supplementary Table 3). On the sea floor, the proportion of Nps-1-4 was significantly higher than in the plankton. These morphotypes had thicker, less transparent tests compared to Nps-5 and the majority of Npd, suggesting that they were individuals that had reached maturity and were either sinking or had reached the sea floor. Npd surprisingly makes up 5.3–6.2 % of assemblages in the sediments at the different stations (average 5.8 %) (Fig. 2; Supplementary Table 3). As in the water column, Nps-4 was the least common morphotype in the sediment (ca. 2.7 %; Supplementary Tables 5–7). We observed that the majority (>90 %) of the Npd group consisted of relatively small, translucent, thin-walled individuals. The remainder (ca. 10 %) comprised a variety of larger morphotypes comparable to Nps-1-4 (Plate 1, Figs. 15–19 and Plate 2, Figs. 16–20).

3.2. Morphometric results

Our AutoMorph measurements of 14,609 individuals (12,896 water column, 11,713 sediment) include test area (μm^2), major and minor axis (Supplementary Fig. 2), and aspect ratio, providing biometric support for the morphotype concepts (Fig. 4, Supplementary Table 8). We saw a consistent pattern in morphotype size in both water column and sediment assemblages (Fig. 4), with test size increasing in the following order: Nps-5, Npd, Nps-1, Nps-3, Nps-2, Nps-4. The test area vs. aspect ratio for Nps-1 to Nps-4 occupy similar areas of morphospace for planktonic and sediment environments, with the exception of Npd where we find that water column Npd are all relatively small (test areas

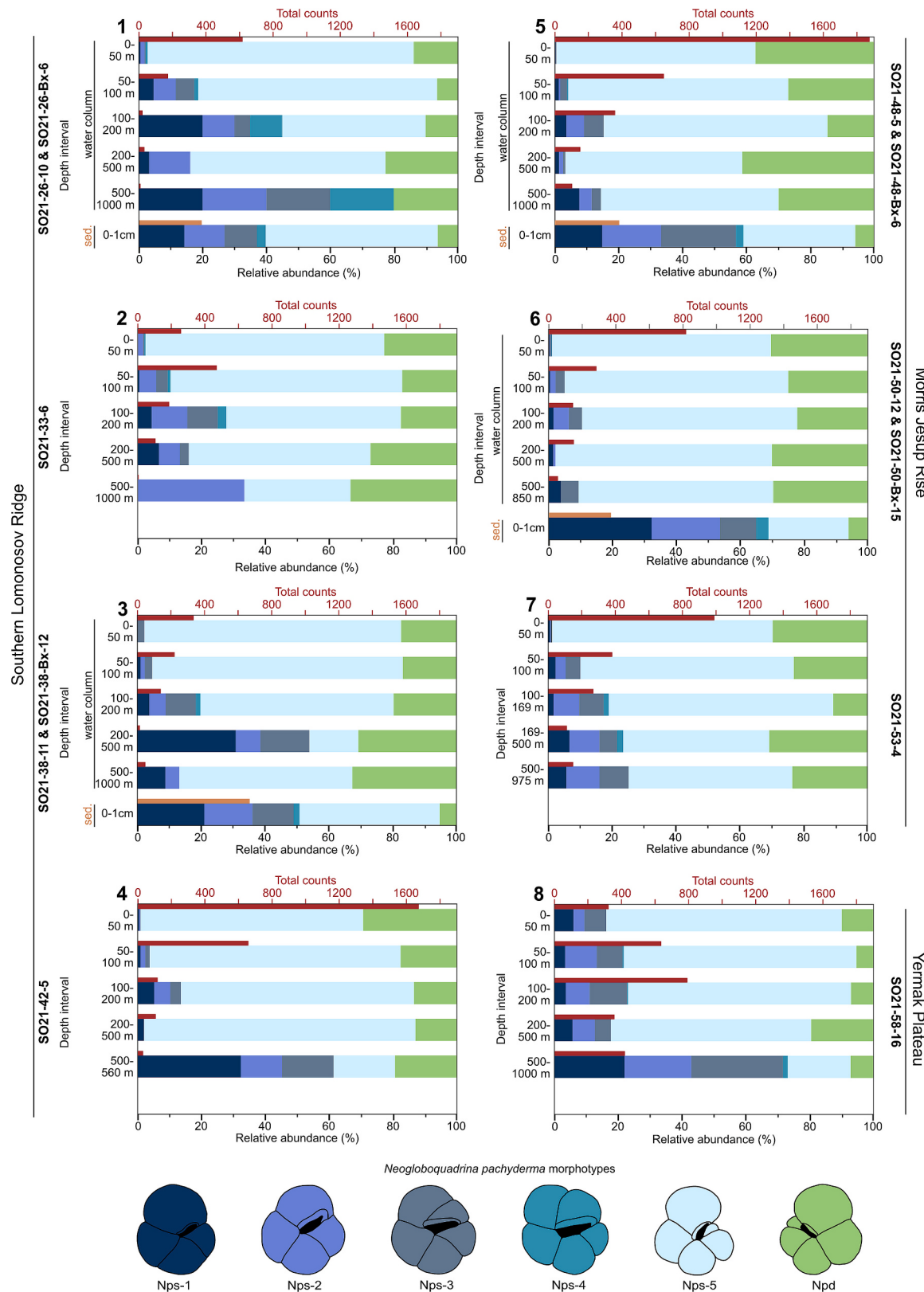


Fig. 2. Stacked bar charts displaying the relative abundance (% of 16,161 specimens) of *N. pachyderma* morphotypes in the 5 vertically distributed multinet depths at the 8 plankton and 4 box core stations (Supplementary Tables 2 and 3). Each morphotype is represented by a distinct colour, with a corresponding cartoon illustrating the morphology. Red bars indicate the total counts for each net and light brown for the surface sediment samples. The total counts for the net samples are based on all specimens found in a net, whereas the sediment sample total counts are based on a minimum of 300 specimens. (For interpretation of the references to colour in this figure legend, the reader is referred to the web version of this article.)

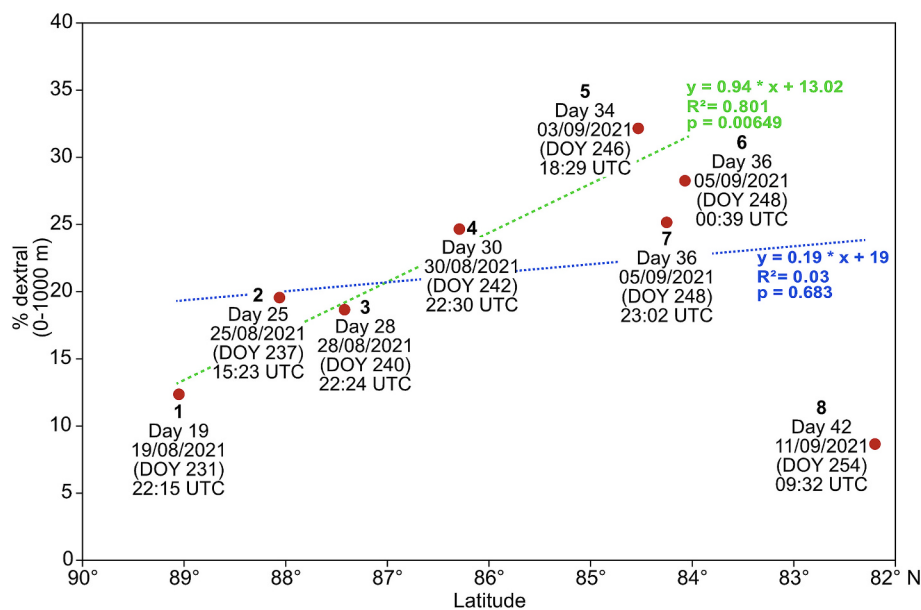


Fig. 3. Relative abundance (%) of right-coiling individuals of *N. pachyderma* (Npd) integrated over 0–1000 m water depth per station across a latitudinal transect. The numbers 1–8 correspond to the station numbers shown in Fig. 1. Cruise day, netting day/date, day of year (DOY), and netting time (UTC) are also indicated. The green dashed line represents the regression of the dataset with Station 8 excluded, while the blue dashed line represents the regression with Station 8 included. The Y, R^2 , and p -values are displayed in the plot. See Supplementary Tables 1 and 4 for additional details. (For interpretation of the references to colour in this figure legend, the reader is referred to the web version of this article.)

ca. $1.1 \times 10^4 \mu\text{m}^2$), compared to the sediment (test areas are mostly $>1.8 \times 10^4 \mu\text{m}^2$; Fig. 4, Supplementary Table 8). We divided the morphotypes into size classes corresponding to life stages often used in palaeoceanographic studies (Supplementary Table 10; see Methods section 2.4): $<80 \mu\text{m}$ (juveniles), $80\text{--}125 \mu\text{m}$ (neanic), $>125 \mu\text{m}$ (mature), and $>150 \mu\text{m}$ (large mature) (Fig. 5 and Plate 3 for immature individuals; see Methods 2.3 for details).

3.2.1. Water column

In the water column (Fig. 5A–H), *N. pachyderma* was most abundant in the $80\text{--}125 \mu\text{m}$ and $>125 \mu\text{m}$ size fractions, except at Station 8, where it was also prominent in the $>150 \mu\text{m}$ size class (Fig. 5H; total counts). Nps-5 was the dominant morphotype across all size classes at all stations, particularly in the $<80 \mu\text{m}$ (73.5–95 %, Supplementary Table 10) and $80\text{--}125 \mu\text{m}$ (68.3–88.01 %, Supplementary Table 10) fractions, which mainly consist of translucent, thin shelled specimens (Plate 3). Similarly, in the Npd category, the translucent Npd morphotype (Plate 3) is also dominant across this same range of size fractions, with relative abundances of 5.00–26.47 % in the $<80 \mu\text{m}$ fraction and 11.13–31.7 % in the $80\text{--}125 \mu\text{m}$ fraction (Supplementary Table 11). Morphotypes Nps-1 to Nps-4 show very low abundances in the water column, especially in the $<80 \mu\text{m}$ and $80\text{--}125 \mu\text{m}$ fractions. These four morphotype are absent in the $<80 \mu\text{m}$ fraction, while only Nps-1 is present in the $80\text{--}125 \mu\text{m}$ fraction in low amounts (<1 %; Supplementary Table 10). The representation of Nps-1 to Nps-4 increases slightly in the $>125 \mu\text{m}$ and $150 \mu\text{m}$ size fractions but remain low compared to Nps-5 and Npd, with relative abundances generally ranging between ca. 4–10 %. Among these, Nps-3 is the most abundant across the stations in the larger size fractions.

The depth distribution of the Nps-5 and Npd size-classes provided insights into the depth habitat of immature and mature forms (Fig. 6, Supplementary Tables 11 and 12). The test size ranges in relation to maturity are discussed in the methods (Section 2.3) and this terminology is applied below. In the upper 0–100 m, Nps-5 was predominantly found as neanic ($80\text{--}125 \mu\text{m}$) individuals (average ca. 53 %; Fig. 6, Supplementary Table 12), followed by mature ($>125 \mu\text{m}$) individuals (average ca. 41.5 %; Fig. 6, Supplementary Table 12), in particular at Stations 1,

2, 4, 5, and 6. In general, juveniles ($<80 \mu\text{m}$) were the least abundant (average ca. 5 %) and only present in the upper 100 m. With increasing depth, the proportion of mature ($>125 \mu\text{m}$) and large mature individuals ($>150 \mu\text{m}$) both increased. At 100–200 m, mature individuals accounted for ca. 58 % on average (with about 34 % of these being large mature). A similar trend continued at 200–500 m, where the population consisted of ca. 67 % mature individuals (with about 40 % of these being large mature). At depths >500 m, Nps-5 populations consisted almost entirely of mature individuals, with around 76 % being mature and about 51 % of these being large mature.

Npd showed a similar trend to Nps-5, with the upper 100 m being dominated by neanic individuals (ca. 55 %; Fig. 6, Supplementary Table 12), followed by mature (ca. 42 %) of which 22 % of these were large mature. Juveniles were only present in the upper 100 m (ca. 3 %), similar to Nps-5 juveniles. The shift towards larger size classes at depth was more pronounced for Npd than for Nps-5. At 100–200 m, the mature population increased to ca. 67 % (about 38 % of these were large mature), while at 200–500 m mature individuals rose to ca. 89 % (about 53 % of these were large mature).

At depths greater than 500 m, Npd became almost exclusively composed mature specimens (ca. 93 %), of these about 72 % were large mature.

Overall, Stations 4–6 had the highest proportions of neanic individuals in the upper 100 m (ca. 50 % in the $80\text{--}125 \mu\text{m}$ size fraction; Supplementary Table 12), while Stations 7 and 8 showed a strong presence of mature specimens at depth ($>125 \mu\text{m}$ averaging ca. 60 %; Supplementary Table 12). The shift from smaller to larger individuals with increasing depth suggests vertical sorting driven by either differential habitats of different growth stages or selective sinking of larger, more mature forms.

In summary, Nps-5 and Npd displayed clear depth-dependent size distributions in the water column, with immature specimens dominating the upper 100 m and larger, mature specimens more abundant at depth. Stations 4–6, which were sampled consecutively between August 30th and September 5th (00:39 UTC) 2021 (Supplementary Table 1), had high concentrations of immature specimens in the upper layers, particularly within the $80\text{--}125 \mu\text{m}$ size fraction. Station 7, also sampled on

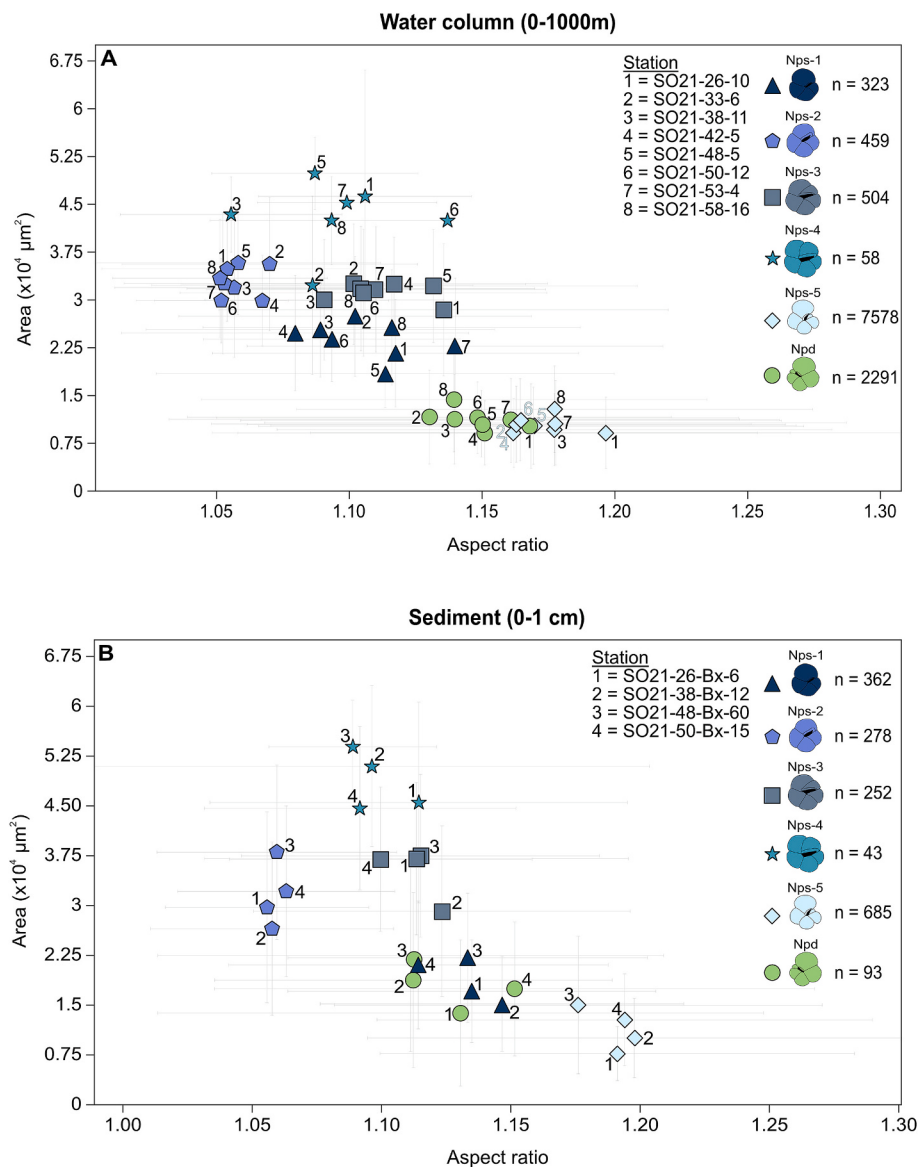


Fig. 4. Mean morphological variables (AutoMorph test area vs aspect ratio parameters Supplementary Table 8) for the predefined *N. pachyderma* morphotypes at all sample stations. (A) water column specimens (all depths combined), and (B) sediment sample specimens. Error bars represent the standard deviation on all specimens for the predefined morphotypes from the $>50 \mu\text{m}$ size fraction. Sample stations are indicated by numbers, the different morphotypes by colour. N values refer to the total number of individuals for each morphotype across all stations, see Table S8 for N values of individuals for each morphotype per station. Test area and aspect ratio values measured from 2D light microscope images using AutoMorph.

September 5th (23:03 UTC), showed a similar pattern but with a high prevalence of larger specimens ($>125 \mu\text{m}$) in deeper layers. Station 8, sampled on September 11th (Supplementary Table 1), recorded a strong deep-water presence of larger, mature specimens, with a less pronounced presence of immature specimens in the upper layers. These spatial and temporal variations point to changes in population life stage composition and vertical distribution, likely linked to the timing of sampling.

3.2.2. Sediment

The sediment assemblages showed a different distribution pattern: while Nps-5 remained dominant in the smaller size fractions (Fig. 5I-L), the larger size fractions ($>125 \mu\text{m}$) were primarily composed of morphotypes Nps-1 through Nps-4 (Fig. 5I-L, Supplementary Table 11). Additionally, small Npd specimens ($<80 \mu\text{m}$) were absent from sediments and the Npd population in general was dominated by larger specimens ($>80 \mu\text{m}$). In summary, netted populations, which were

dominated by small, largely immature individuals ($80-125 \mu\text{m}$) with an unusually high proportion of dextral forms (up to 32.3 %), contrasted markedly with sedimented assemblages especially in regards to the abundance of morphotypes Nps1-Nps-4 (i.e. mature individuals).

3.2.3. Proloculus size

Recent work on the life cycle of *N. pachyderma* (Darling et al., 2023; Meiland et al., 2022, 2024) highlight the importance of examining both test morphology and proloculus size to reveal the different reproductive stages of the *N. pachyderma* life cycle. To shed light on the *N. pachyderma* Type Ia reproductive cycle in the CAO, we measured external proloculus diameter on SEM images of 231 randomly picked Nps-5 and Npd specimens from Station 4, 0–50 m water-depth, using a modified approach to that of Darling et al. (2023) and Meiland et al. (2024) (Fig. 7, Plate 4, Supplementary Table 13). The mean external diameter of Nps-5 ($n = 117$) was $18.2 \mu\text{m}$ compared with Npd, which was $12.8 \mu\text{m}$ ($n = 114$). Gaussian Mixture Model (GMM) analysis shows that the distribution was

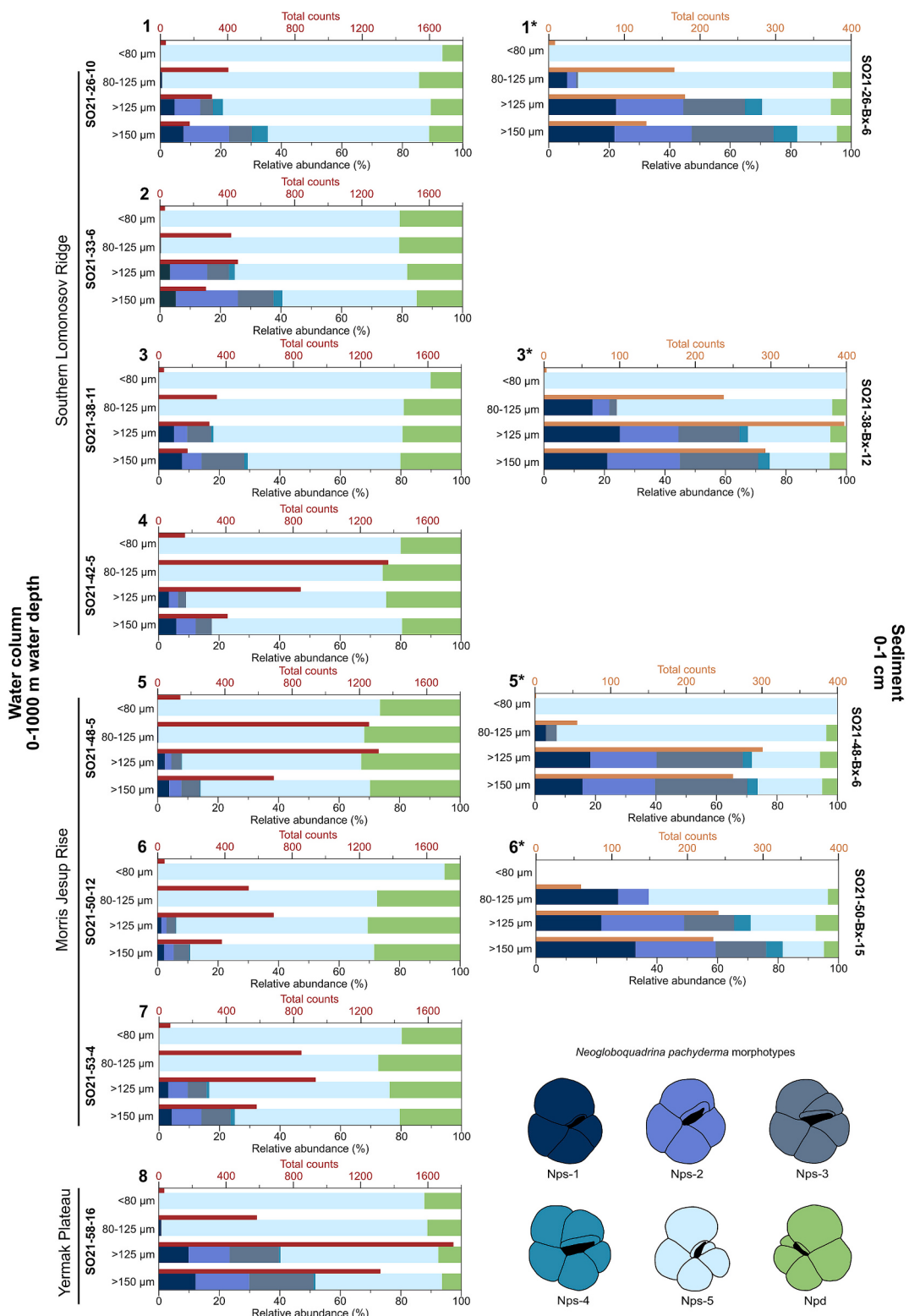


Fig. 5. Stacked bar charts displaying the relative abundance (%) of 12,896 water column and 1713 sediment specimens) of *N. pachyderma* morphotypes categorised into 4 pre-defined size classes (<80, 80–125, >125, >150 µm) at 8 multinet stations (A-H) and 4 box-core stations (I-L), with each morphotype represented by a distinct colour in the illustrations. Red bars indicate the total counts for each net and surface sediment sample. The numbers 1–8 correspond to the station numbers shown in Fig. 1. Stations marked with an * are box core stations. See Supplementary Tables 9 and 10 for more details. (For interpretation of the references to colour in this figure legend, the reader is referred to the web version of this article.)

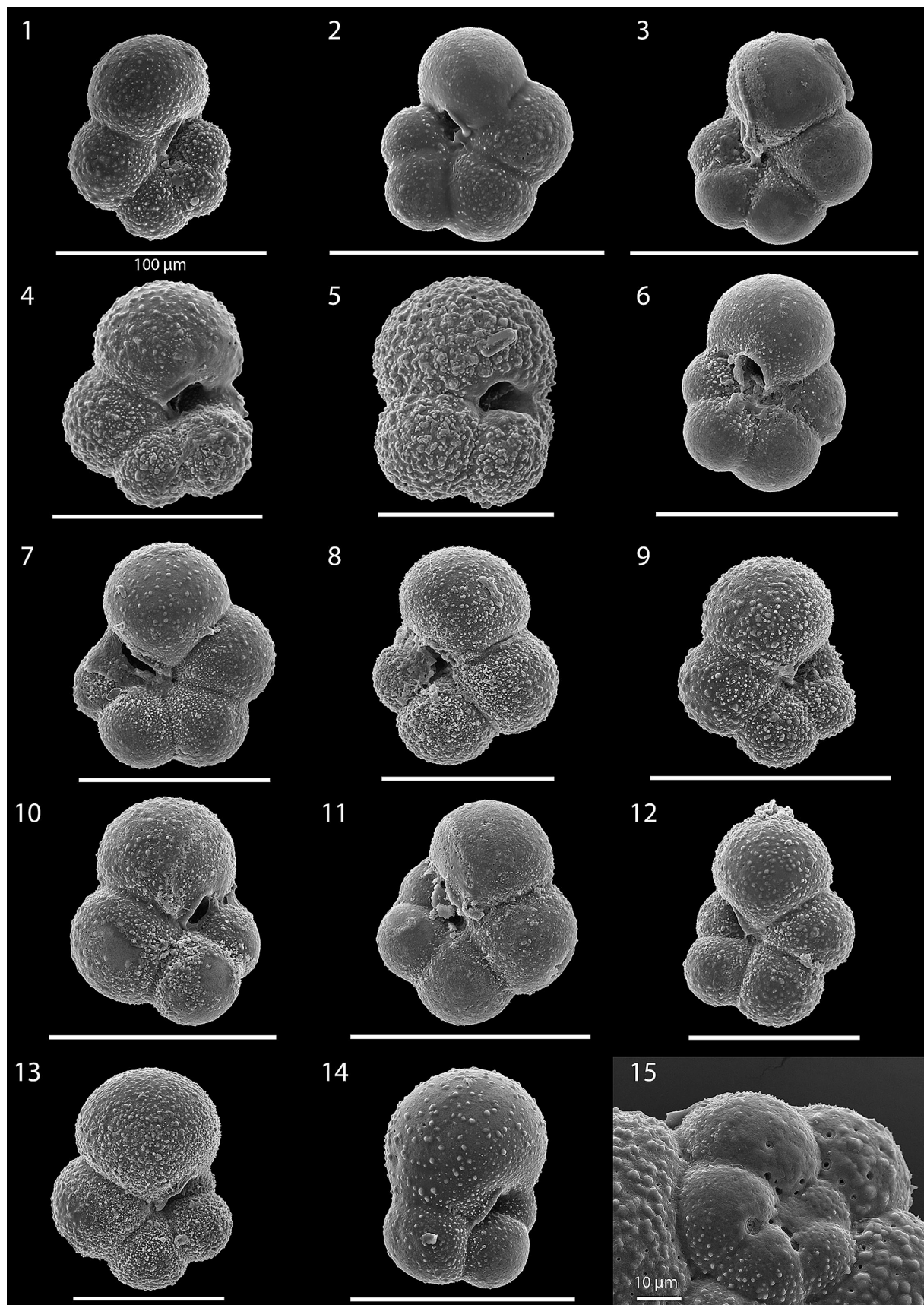


Plate 3. Examples of subadult Nps-5 and Npd individuals from the water column and sediment. 1 Nps-5 (SO21-48-Bx-6, 0–1 cm), 2, 3 Npd (SO21-38-11, 0–50 m), 4, 5 Nps-5 (SO21-53-4, 50–100 m), 6–7 Npd (SO21-53-4, 50–100 m), 8 Npd (SO21-50-12, 0–50 m), 9 Nps-5 (SO21-50-12, 0–50 m), 10 Nps-5 (SO21-26-10, 0–50 m), 11, 12 Npd (SO21-26-10, 0–50 m), 13, 14 Nps-5 (SO21-58-16, 100–200 m), 15 Spiral side of Npd showing the first whorl with pores in the sutures and pores moving towards the inner chamber in the second whorl (SO21-50-12, 0–50 m). All scalebars are 100 µm, unless otherwise indicated.

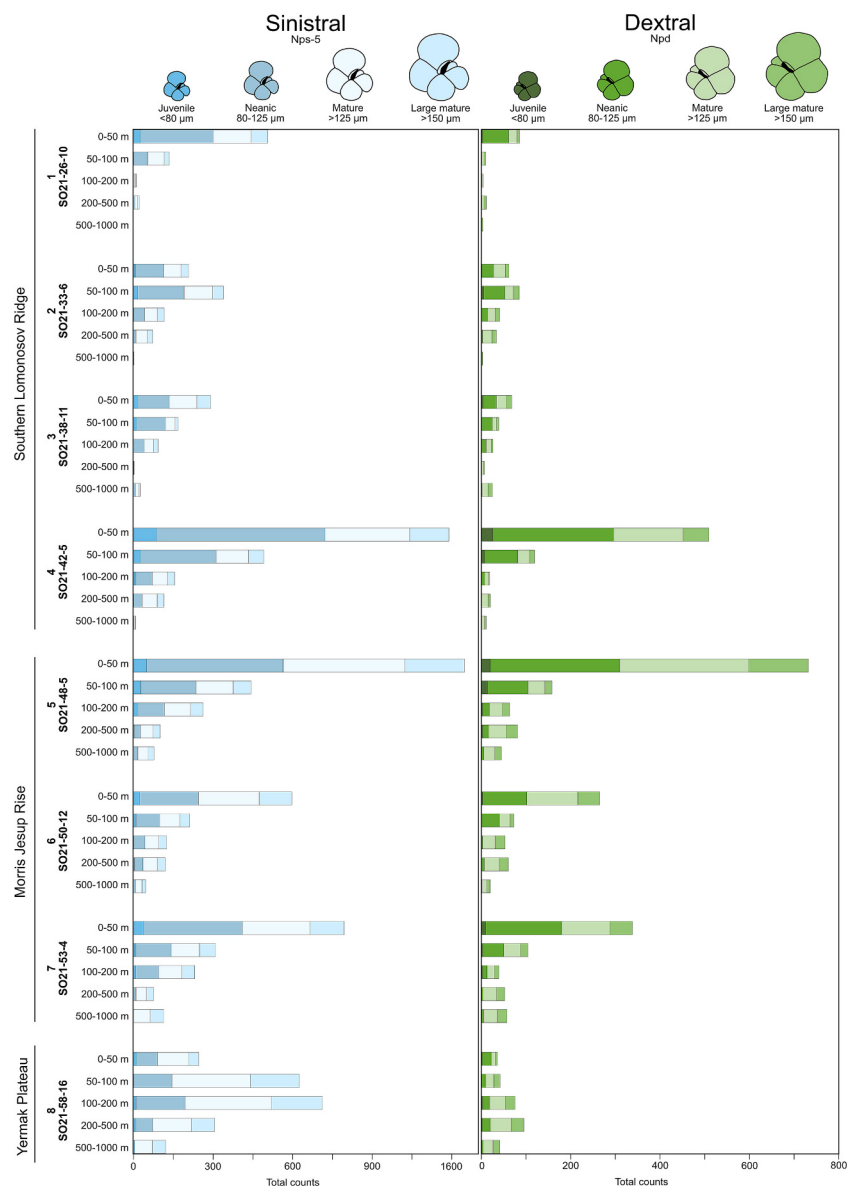


Fig. 6. Stacked bar charts displaying station-specific abundance patterns of the *N. pachyderma* Nps-5 and Npd morphotypes through the water column broken into test size classes (<80, 80–125, >125, >150 µm). Each of the 4 size classes represented by a distinct colour shade. The numbers 1–8 correspond to the station numbers shown in Fig. 1. See Supplementary Tables 11 and 12 for more details.

bimodal in the sinistral dataset (Nps-5) (best-fit mean likelihoods $\mathcal{L}_{\text{sinistral}}^{k=2} = -374.63$, where k is the number of components), with two distinct components and equal probabilities of belonging to each component ($\lambda = 0.5$) (Fig. 7B, Table 2). For the dextral dataset the distribution was also bimodal ($\mathcal{L}_{\text{dextral}}^{k=2} = -291.36$) but with one dominant component (Fig. 7A; $\mu = 11.92$, $\lambda = 0.93$) and a small probability of an individual belonging to the larger proloculus group ($\mu = 24.90$, $\lambda = 0.07$).

4. Discussion

4.1. Morphotype distribution and the reproductive strategies of *N. Pachyderma*

All six *N. pachyderma* morphotypes recognised in this study were present in both the CAO water column and corresponding seafloor sediments, although their relative abundances and size distributions varied between these two environments (Figs. 3, 5, 6). Individuals were

assigned to morphotypes visually, a classification supported by the distribution of corresponding morphologic variables. Plots of test area vs. aspect ratio for Nps-1 to Nps-4 define consistent areas of morphospace in our scatter plots for planktonic and sediment environments (test area vs. aspect ratio; Fig. 4). This suggests that the morphological characteristics used to define each morphotype are consistently applied between the water column and seafloor, with most morphotypes in the water column eventually settling to the seafloor, albeit in different relative proportions (Fig. 2). The exception is Npd, which appear much smaller in the water column (test areas ca. $1.1 \times 10^4 \mu\text{m}^2$) compared to the sediment, where Npd individuals are generally larger (on average $1.8 \times 10^4 \mu\text{m}^2$) (Fig. 4; Supplementary Table 8). We interpret this size difference as evidence that no ‘mature’ (larger) Npd individuals were present in the water column at the time of sampling. This suggests that the small, abundant Npd observed represent a relatively recent reproductive cohort, likely produced during an ongoing and temporally restricted central Arctic summer bloom period. Although the Nps-5 and Npd morphologies appeared similar (small and translucent) in both the

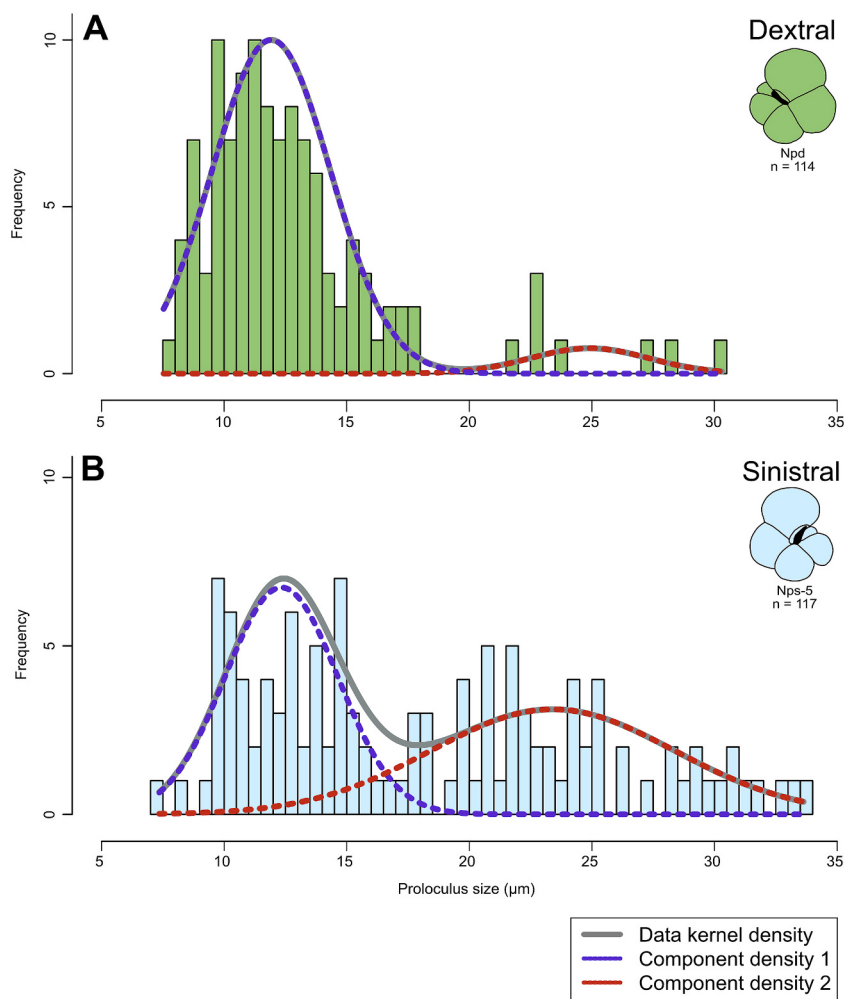


Fig. 7. Kernel and component densities of proloculus diameter data (Supplementary Table 13) and GMM fitting results. (A) Dextral dataset; (B) Sinistral dataset. Histograms of the underlying data separated into 5 µm bins are plotted in light blue beneath the corresponding kernel (grey) and component (blue, red) densities. Note that the component densities are not identifiable (i.e., component density 1 is not necessarily the 'same' component across analyses) and are numbered here for convenience of visualisation. (For interpretation of the references to colour in this figure legend, the reader is referred to the web version of this article.)

water column and the sediment, this similarity does not necessarily indicate that they represent the same developmental or reproductive stage of *N. pachyderma* (discussed below).

For comparison, previously published test size estimates of *N. pachyderma* morphotypes (Eynaud et al., 2009; El Bani Altuna et al., 2018) show similar overall trends in relative size progression from Nps-1 to Nps-4, with Nps-5 consistently smaller. However, absolute mean test sizes differ from our measurements (e.g. Nps-1: 165.2 µm in this study (Table 1) vs. ca. 205 µm in Eynaud et al., 2009), likely due to differences in morphometric methodology, or regional population variability. Aspect ratio values also differ slightly between studies, for instance, we report Nps-2 with an aspect ratio of 1.06 (Table 1) compared to 0.95 ± 5 in El Bani Altuna et al. (2018). These differences underscore the influence of imagine technique, methodology, resolution, and classification thresholds, yet the consistency in relative morphotype proportions across studies supports the robustness of the morphotype framework.

4.1.1. Water column: distribution of life stages

Using test size as a proxy for maturity/life stage (Davis et al., 2020), it can be concluded that juvenile specimens (<80 µm; Nps-5 and Npd) constitute a very small component of our samples. This is likely a consequence of mesh size limitations; even with the fine 55 µm net used in this study, many juvenile tests are likely lost (Fig. 6, Supplementary Table 12). Neanic specimens (immature) (80–125 µm, categorised as

Nps-5 and Npd) were the most abundant size class in the upper 100 m, particularly within the top 0–50 m (Fig. 6, Supplementary Table 12). Their abundance progressively decreased with increasing depth and were largely absent below 500 m. As no specific stains or molecular methods were used to distinguish living from dead specimens, some of the specimens may represent recently deceased or sinking forms.

The distribution of larger individuals at greater depths, particularly at Stations 7 and 8, is consistent with a preferential sinking of mature/adult forms. These individuals likely descend to deeper waters prior to gametogenesis, where they add their gametogenic calcite and subsequently release gametes. Gamete release has yet to be observed in the natural environment, so the precise timing and depth of reproduction remain uncertain. It is also possible that some of these mature/adult forms fall out of the water column without reproducing (Meilland et al., 2022). Stations 4–6 proportionately showed higher surface abundances of smaller individuals, suggesting the population included a wider range of life stages.

The larger morphotypes, comprising heavily encrusted morphotypes Nps-1 through Nps-4, constitute a minor component of the water column (ca. 10 %). Their high level of calcification indicates that they have reached maturity and most likely reproduced sexually, consistent with culture observations showing that tests thicken prior to gamete release in the sexually reproducing generation (gamonts; Darling et al., 2023). These findings are further supported by encrustation analyses from

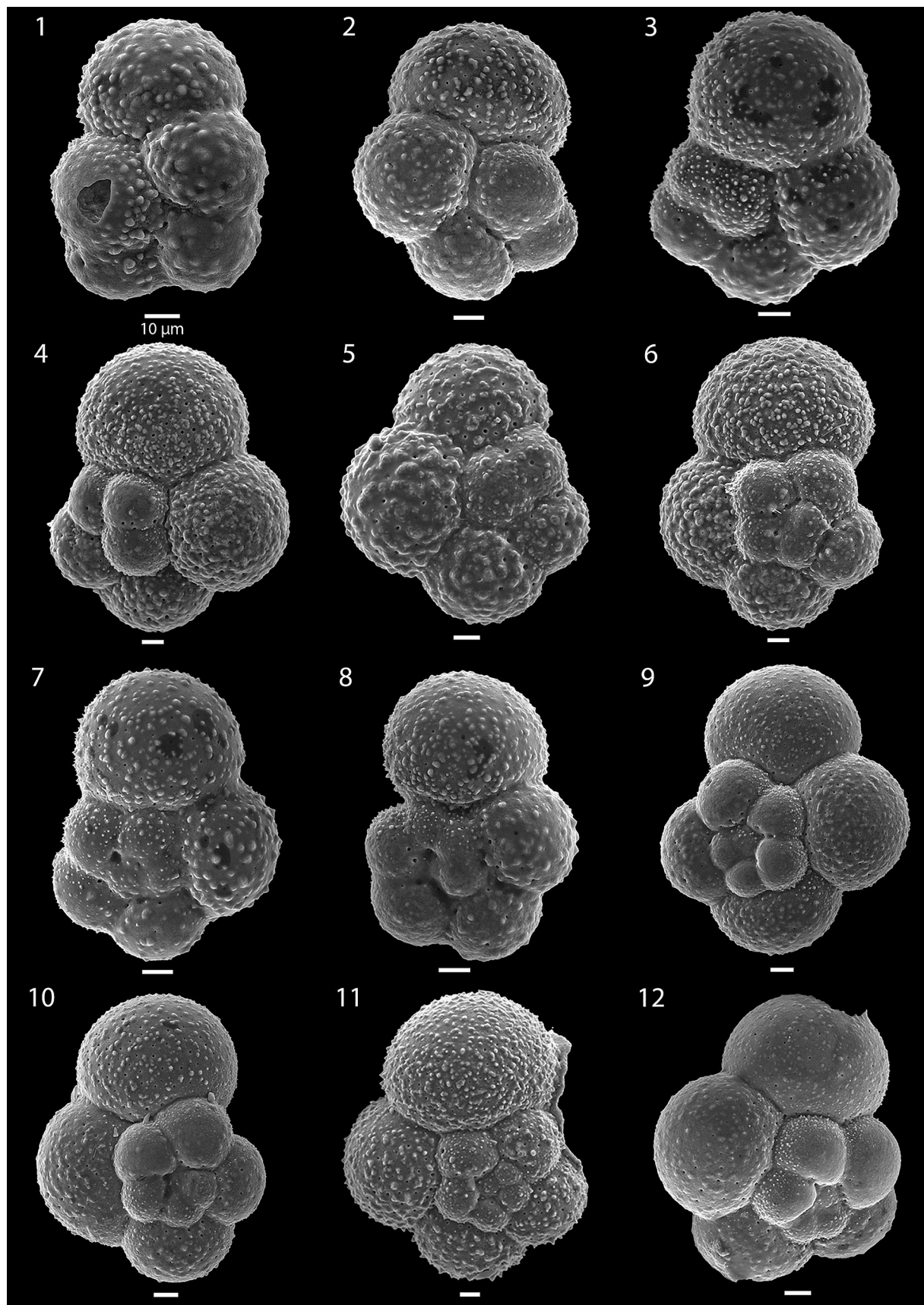


Plate 4. Examples of proloculus size variability of dextral (Npd) and sinistral (Nps-5) *N. pachyderma* from SO21-42-5, 0–50 m. 1–5 largest proloculi, 6–8 small proloculi, 9–12 smallest proloculi. All scalebars are 10 µm unless otherwise indicated.

Table 2

Gaussian mixture model parameters for proloculus size (μm) for sinistral and dextral datasets from specimens collected at Station SO21-42-5, 0–50 m water depth (Supplementary Table 13). See [Plate 4](#) for examples of the three proloculus sizes.

Dataset	# components (best-fit)	Component identifier (cf. Fig. 7)	Means (μm)	Standard deviations (σ)	Weights (λ)
Dextral	2	Blue	11.92	5.87	0.93
		Red	24.90	5.87	0.07
Sinistral	2	Blue	12.34	5.30	0.5
		Red	23.40	24.68	0.5

natural populations in the Barents Sea, which document increased shell calcification (gametogenic calcification) with depth and infer reproduction in *N. pachyderma* based on these features ([Ofstad et al., 2021](#)).

The predominance of small (55–125 μm), weakly calcified Nps-5 and Npd morphotypes in the water column (0–500 m) indicates that they are immature specimens that have not yet reproduced and that could eventually mature into one of the other morphotypes. We propose that the larger (>125 μm) Nps-5, and Npd observed in the water column, represent sinistral and dextral mature specimens that may reproduce asexually. This interpretation is based on *N. pachyderma* culture studies in which no Npd has been observed to release gametes, suggesting that reproduction in Npd is exclusively asexual ([Kimoto and Tsuchiya, 2006](#); [Meilland et al., 2022](#)).

Observations from the Barents Sea also report low-density *N. pachyderma* tests, interpreted to be similar to our thin shelled Nps-5, throughout the entire water column ([Ofstad et al., 2021](#)), supporting the idea that thin-shelled individuals persist at depth. However, not all will successfully reproduce and many thin-walled specimens will accumulate in the sediments. In fact, [Meilland et al. \(2022\)](#) estimated that 54 % of a *N. pachyderma* population die without ever reproducing, reinforcing the interpretation that many thin-walled individuals ultimately sink and accumulate on the seafloor, even in the absence of reproductive success.

In culture studies individuals, individuals producing live offspring had attained test sizes >125 μm and remained thin-shelled and translucent following asexual reproduction events ([Davis et al., 2020](#); [Meilland et al., 2022](#)). The offspring, however, have been observed to develop thicker walls resembling morphotypes, including dextral variants, of Nps-1 through Nps-4, as seen in [Fig. 5](#) of [Davis et al. \(2020\)](#). [Davis et al. \(2020\)](#) note that generations of *N. pachyderma* could be described as isomorphic i.e. parent and offspring appear very similar in shape and form, although the potential morphometric differences between parent (thin-shelled Nps-5) and offspring (encrusted Nps-1 to Nps-4 and their dextral equivalents) merit further study, as the mechanisms underpinning these differences remains unclear. Even though sinistral and dextral morphotypes can appear morphologically similar ([Plates 1 and 2](#)), they differ in their reproductive pathways, which will be discussed in the following sections.

4.1.2. Proloculus size categories and life-stage interpretation

To interpret life-stages in *N. pachyderma*, it is important to clarify the terminology used for proloculus size of the different generations found specifically in *N. pachyderma*, since they do not follow the “classic” megalospheric (asexual) and microspheric (sexual) test descriptions observed in some benthic foraminifera ([Goldstein, 2002](#)). Moreover, [Goldstein \(2002\)](#) demonstrated that there is nothing typical about the life cycles of benthic foraminifera and many do not conform to the so-called ‘classic pattern’. Although the non-spinose planktonic foraminifera clearly evolved from the rotaliid group of benthic foraminifera ([Holzmann and Pawłowski, 1996](#); [Morard et al., 2024](#)), the reproductive cycles of their sister benthic clades have yet to be studied. Additionally, it is important to note that the spinose and microperforate planktonic foraminifera groups are not closely related to the non-spinose group and

do not represent sister clades ([Morard et al., 2024](#)).

To simplify interpretation, we define three operational categories based on proloculus size derived from our GMM results and previous studies ([Meilland et al., 2022](#); [Darling et al., 2023](#)): (1) large, associated with agamonts (mean 18.8 μm), (2) medium, associated with gamonts (mean 16.6 μm), and (3) small (approximately 12 μm ; [Table 2](#)), associated with specimens of currently unresolved reproductive origin. While these ranges overlap and show wide variation ([Table 2](#)), they provide a practical framework for assigning likely life stages, especially in the lack of direct reproductive observations in wild populations.

For clarity and consistency, we refer to these size classes as Large, Medium, and Small proloculus categories throughout this section. These terms are used as descriptive labels within the context of this study to distinguish our terms from those of other studies, rather than as empirically defined classes. These classes form the basis for interpreting the statistical distributions described below.

Interpretation of proloculus size distribution begins with dextral *N. pachyderma* (Npd), which we propose is composed of only two reproductive stages. Agamonts and schizonts have been shown to coil in either direction ([Darling et al., 2023](#); [Meilland et al., 2022, 2024](#)), whereas gamonts are consistently reported as sinistral in culture studies ([Kimoto and Tsuchiya, 2006](#); [Meilland et al., 2022](#)), and thus are not expected to occur among dextral individuals. The Npd dataset, therefore, is restricted to agamonts (Large), and individuals of currently unknown origin (Small), which we tentatively interpret as schizonts.

The proloculus size distribution in the Npd dataset ([Fig. 7A](#)) exhibits a clear bimodal distribution, as resolved through GMM. Two well-separated peaks are evident: the red density component, centred at approximately 24.9 μm , and the blue component, centred at approximately 11.9 μm ([Table 2](#)). These size classes are interpreted to represent agamonts and schizonts, respectively, based on comparisons with previous studies and size ranges observed in literature ([Meilland et al., 2022](#); [Darling et al., 2023](#)). The average proloculus size values under the red curve in this study (24.9 μm ; [Table 2](#)) are higher than the CT scanned ([Darling et al., 2023](#)) or culture experiment ([Meilland et al., 2022, 2024](#)) values for agamonts. This discrepancy is most likely due to the other studies using internal CT scans or measurements of thin-walled specimens immersed in oil, which enhances visualisation, whereas our proloculus sizes were measured externally. Despite such discrepancies, the size separation between life stages remains robust across datasets as shown in the distinct density components.

The two-component interpretation in the Npd population provides a useful comparative framework for evaluating the more complex sinistral population (Nps-5), which is expected to contain three distinct reproductive stages: gamonts, agamonts, and schizonts. The GMM applied to the sinistral dataset ([Fig. 7B](#)) also reveals a bimodal distribution, with the red and blue density components spanning a broad range of proloculus sizes and showing an overlap in density around 16 μm . However, given the presence of an additional gamont reproductive stage in the Nps-5 population, the biological interpretation of these statistical modes is more complex.

The blue component in Nps-5 ([Fig. 7B](#)) has a mean proloculus size of approximately 12.3 μm , nearly identical to the blue component in the dextral population (11.9 μm , [Table 2](#)). This similarity supports the interpretation that the blue density component in both datasets corresponds to schizonts. The red component in the Nps-5 dataset ([Fig. 7B](#)), by contrast, covers a broader range of sizes and includes values consistent with both gamonts and agamonts. Proloculus sizes reported in the literature indicate that gamonts typically range around 16.6 μm , while agamonts are somewhat larger (mean 18.8 μm) ([Meilland et al., 2022](#); [Darling et al., 2023](#)). Notably, the blue component tapers into the red component range, with a relatively high frequency of specimens around 16 μm where these two components overlap. This overlap suggests that gamonts are present in both components, as they may be produced by both agamonts and schizonts (e.g. [Darling et al., 2023](#); [Meilland et al., 2024](#)). Consequently, although GMM resolves a bimodal distribution

statistically, the underlying biological assemblage in Nps-5 comprises three distinct life stages: (1) schizonts (blue component, $\sim 12.3 \mu\text{m}$), (2) gamonts (overlapping region, $\sim 16 \mu\text{m}$), and (3) agamonts (red component, $23.4 \mu\text{m}$). The overlap in blue and red components at $\sim 16 \mu\text{m}$ aligns closely with reported gamont proloculus sizes from Baffin Bay (Meilland et al., 2022), supporting that the Nps-5 data represents a three-component assemblage, as the red curve includes size values consistent with those for both gamonts (mean $16.6 \mu\text{m}$) and agamonts (mean $18.8 \mu\text{m}$) (Meilland et al., 2022; Darling et al., 2023).

This more complex three-stage structure in Nps-5 stands in contrast to the Npd population, which contains only two reproductive stages, the agamont and the schizont, each corresponding directly to one of the statistically resolved modes (Table 2). Thus, although both Npd and Nps-5 show bimodal distribution in proloculus size, the underlying biological composition differs. Comparing these two populations provides a useful framework for interpreting the Nps-5 dataset with greater confidence, using the simpler Npd distribution as a reference to assign life stages to the overlapping proloculus size classes observed in Nps-5 gamonts. Thus, the apparent bimodality of the proloculus size distribution reflects a more complex three-stage biological structure that cannot be fully resolved by statistical modelling alone.

Additional support for the presence of multiple life stages comes from population structure dynamics. Agamonts typically produce over 250 gamont offspring each (Kimoto and Tsuchiya, 2006; Meilland et al., 2022, 2024). This reproductive output leads to a population structure in which gamonts vastly outnumber their agamont parents in the water column. Consequently, sinistral gamonts are expected to dominate the water column assemblage, with sinistral agamonts comprising only a small fraction. Based on this expectation, the Nps-5 agamonts likely account for less than 3 % of the total assemblage, falling within the lower tail of the red density curve in Fig. 7B (Darling et al., 2023). This interpretation is strongly supported by the low numbers of dextral agamonts observed beneath the red curve in Fig. 7A.

It should be noted that in the water column data set in this study, proloculus diameter measurements were confined to Nps-5 and Npd due to method practicalities (Plate 4). As discussed above, the water column Nps-5 assemblage includes agamonts (Large), gamonts (Medium) and specimens of currently “unknown” origin with a small proloculus, hypothesised to be schizonts (Small). The Npd assemblage includes agamonts (Large) and the “unknowns” (Small). The proloculus size in the larger heavily encrusted mature morphotypes Nps-1 through Nps-4 was not assessed in this study, as limitations in our SEM method prevented accurate identification of proloculi in these heavily encrusted morphotypes. Although this could be facilitated with future micro-CT imaging, to which gametogenic calcite is no obstacle, as demonstrated by Ofstad et al. (2021) and Darling et al. (2023), who used this technique to visualise internal chamber structures including the proloculus, these morphotypes would only contribute marginally to the three proloculus size values.

In the Nps-5 dataset, specimens with a small proloculus make up 50 %, while they account for 97 % of the Npd dataset (Table 2). Meilland et al. (2022) similarly reported the presence of specimens with a comparably small proloculus as a minor component within a predominantly sinistral coiling assemblage. In their study, less than 4.5 % of the Greenland Sea population exhibited a small proloculus, while in Baffin Bay, confirmed small proloculus specimens comprised less than 3.47 %, with 20.46 % remaining unassigned due to significant overlap with the medium proloculus size range. While direct confirmation of schizont identity remains unavailable, the recurring presence of this size class in both sinistral and dextral populations supports the hypothesis that it most likely represents a third, previously undercharacterised, asexual schizont generation.

4.1.3. Sediment: Distribution of life stages

The larger, heavily encrusted morphotypes (Nps-1 through Nps-4) constitute a minor component of the water column (ca. 10 %) but

typically make up about 55 % (Supplementary Table 3) of the sediment (0–1 cm depth). Their level of calcification (gametogenic calcification) indicates that they have reached maturity and reproduced sexually (i.e., gamete release), consistent with culture observations showing that tests thicken prior to gamete release in sexually reproducing generations (gamonts; Davis et al., 2020; Meilland et al., 2024). The encrusted and larger morphotypes of Nps-1 to Nps-4 average 54.6 % across all box core samples (Supplementary Table 6).

The Nps-5 component in the underlying sediments include a higher proportion of larger individuals ($>125 \mu\text{m}$) compared to the water column (Fig. 5). These would include a small number of mature agamonts, that would have reproduced asexually (Darling et al., 2023), since they are thin walled, with test sizes $>125 \mu\text{m}$ (Meilland et al., 2022, 2024). However, these would represent <3 % of the sediment assemblage, since they are likely to occur in equivalent numbers to the Npd agamonts in the water column (3 %; Meilland et al., 2022; Darling et al., 2023). By far the largest sediment Nps-5 component is represented by the gamont population that failed to grow or reproduce at maturity. In addition, in these Arctic waters there will be a smaller component of Nps-5 that represents the “unknowns” with the Small proloculus shown to be present in the water column in Fig. 7A.

A similar equivalent increase in Npd above the 3 % value would also be expected, since the “unknowns” with the Small proloculus are also observed to exhibit dextral coiling (Fig. 7A). How large this additional component would be would depend upon how often they are produced over the seasonal cycle. If they are rarely produced, they would not influence the Arctic coiling percentages in core tops, since these central Arctic sediments represent millennia of accumulation (e.g. Backman et al., 2004). However, Arctic core tops exhibit marginally higher percentages of dextral coiling (ranging from 2 % to 9.1 %, based on varying sieve mesh sizes ($>63 \mu\text{m}$ - $>150 \mu\text{m}$); this study and El Bani Altuna et al., 2018; Nørgaard-Pedersen et al., 2007; Prabhakar et al., 2024) compared to other regions further south, such as Baffin Bay (4 %; Knudsen et al., 2008) and the Greenland Sea (<3 %; Bauch et al., 2003), although in these regions *N. incompta* starts to encroach, making the differentiation from Npd more problematic.

4.2. Dextral coiling and the schizont hypothesis: evidence for an additional asexual generation in *N. pachyderma*

In both the CAO water column and underlying sediment samples, we find higher proportions of dextrally coiled individuals than expected, compared to the <3 % dextral coiling ratio described in Darling et al. (2006, 2023). Plankton sampling in the Nansen Basin water column had previously found *N. pachyderma* dextral in proportions up to 6.2 % (net mesh $63 \mu\text{m}$; Carstens J. and Wefer, G., 1992). However, our observations show an even greater divergence from the commonly referenced 3 % coiling guideline, suggesting that higher dextral coiling values in the CAO may differ from those traditionally assumed for other regions. Dextral coiling values were consistently well above 3 % and rise as high as 32.3 % (Supplementary Table 5) in the water column. We propose that these results represent an additional asexual event in the reproductive cycle of *N. pachyderma*, which may be specific to the CAO and involve a third, clonal pathway known as the schizont cycle.

Several culture studies have demonstrated that aberrant coiling is a signal of asexual reproduction in *N. pachyderma* (Kimoto and Tsuchiya, 2006; Kimoto and Tsuchiya, 2006; Davis et al., 2020; Meilland et al., 2022, 2024), where offspring are released as opposed to gametes. This process forms part of a generational alternation between gamonts (which release gametes) and agamonts (which produce live offspring). While the extent to which asexual reproduction dominates the life cycle of *N. pachyderma* remains debated (e.g. Meilland et al., 2022; Darling et al., 2023), recent culture studies suggest that asexual reproduction may be more common than previously assumed (Meilland et al., 2022, 2024).

Agamonts are rare in the water column and can be either sinistral or

dextral (Meilland et al., 2022, 2024). Following evidence from the rotaliid benthic foraminiferal clades, the offspring are produced by multiple fission following an initial meiotic division, as outlined in Goldstein (2002) and Darling et al. (2023). Their offspring constitute the water column assemblages which are all sinistral coiling haploid gamonts. A proposal for the complete cycle is shown in Darling et al. (2023). As previously noted, the Large (mean 18.8 μm) and Medium (mean 16.5 μm) proloculus sizes correspond to the agamont and gamont generations respectively (Darling et al., 2023; Meilland et al., 2022, 2024). Our dataset (Fig. 7A and B) indicates a potential third component, where specimens with a Small proloculus constitute 50 % of the Nps-5 dataset and 93 % of the dextral dataset (Table 2). We propose that the Small proloculus size, shown under the blue curve in both Nps-5 and Npd (Fig. 7), do not constitute part of the dominating alternation of sexual and asexual generation cycle, but rather represent a clonal schizont reproductive cycle.

Previous studies on the distribution of proloculus size in *N. pachyderma* in the Greenland Sea, and particularly in Baffin Bay, have provided evidence of bimodality (Meilland et al., 2022). In Baffin Bay, the smaller proloculus specimens (ranging 2–16 μm) were classified as microspheric, while those larger than this were classified as megalo-spheric, though these included both gamonts and agamonts (Meilland et al., 2022; Darling et al., 2023). A considerable overlap exists between these two groups, which aligns with the overlap seen between the Nps-5 blue and red curves in this study (Fig. 7B). However, all gamonts (Medium proloculus) in the water column exhibit sinistral coiling, as no dextral-coiling specimens have been observed releasing gametes in culture (Davis et al., 2020; Meilland et al., 2022, 2024). This is further supported by their absence in the Npd curve (Fig. 7A), which only includes the Small and Large proloculus groups. Consequently, the Small proloculus group stands apart in the Npd curve, displaying the full, unobscured range of proloculus sizes characteristic of this category. These sizes also closely match those represented under the blue curve in the Nps-5 dataset (Fig. 7B), indicating their clear commonality.

4.2.1. Evidence for clonal schizont reproduction in *N. pachyderma*

Meilland et al. (2024) observed a deviation from the primary alternating generation cycle in their *N. pachyderma* cultures, where agamonts produce the sinistral coiling water column assemblages (Meilland et al., 2022; Darling et al., 2023). They found that successive generations may be produced by multiple fission, a possibility originally suggested by Darling et al. (2023). However, it is important to define what is meant by the process of multiple fission. In some groups of benthic foraminifera, meiotic reductive division (which increases genetic variation in gamont offspring) precedes multiple fission in the agamont (Le Calvez, 1946, 1950; Grell, 1954; Arnold, 1955; Goldstein, 2002). This asexual stage in benthic foraminifera is therefore not clonal as in many other organisms, but rather a reductive division from diploid to haploid cells. However, when successive generations of multiple fission are observed, as documented by Meilland et al. (2024), it is highly likely that clonal multiple fission without meiosis is occurring, since this phenomenon is regularly observed as a facultative third component of the life cycle of benthic rotaliids (e.g. Leutenegger, 1977; Dettmering et al., 1998; Goldstein, 2002).

Our analysis of the life cycle of *N. pachyderma* is derived from a combination of both benthic and non-spinose planktonic foraminiferal literature, consistent with the position of meiosis within the benthic foraminiferal clades (Goldstein, 2002; Goetz et al., 2022). All three components – the sexual gamont generation (Meilland et al., 2022), the asexual agamont generation (Meilland et al., 2022; Darling et al., 2023), and the asexual clonal schizont generation (hypothesised by Darling et al., 2023 and observed by Meilland et al., 2024) – have now been suggested to occur in *N. pachyderma*'s life cycle in its natural environment, based on this study. The question remains how the three components (Large, Medium, and Small) we have identified in proloculus size distribution in this study relate to the three distinct reproductive

pathways observed in the *N. pachyderma* life cycle. It has been established that the agamonts have a Large proloculus (sinistral and dextral) and the gamonts have a Medium size proloculus (sinistral), though both have a wide range of variation (Meilland et al., 2022; Darling et al., 2023). This leaves the Small proloculus group (both sinistral and dextral coiling), which have mean proloculus size values (Table 2) of 12.34 μm (sinistral) and 11.92 (dextral) with a standard deviation of 5.3 μm and 5.87 μm , respectively, as candidate schizonts. The Small proloculus group are responsible for the higher dextral coiling ratios observed in our water column assemblages. This similarity between the sinistral and dextral GMM results supports our hypothesis that the Small proloculus dataset represents individuals produced by the clonal schizont cycle.

4.2.2. Culture-based support for schizont activity in *N. pachyderma*

Culture studies on *N. pachyderma* (Type IIIa; as defined by Morard et al., 2024) from the Northeast Pacific observed asexual reproduction with offspring released from parent tests, some of which grew to full size and later released gametes (Davis et al., 2020; Kimoto and Tsuchiya, 2006). Kimoto and Tsuchiya (2006) described a dextral agamont producing sinistral offspring (genotyped) of which three produced gametes, which aligns with the primary alternation of generation life cycle. However, Davis et al. (2020) observed a sinistral agamont (thin walled) producing both dextral (35 %) and sinistral (65 %) offspring in a single reproductive event. Their offspring assemblage resembles the composition of the Small proloculus assemblage observed in the water column assemblage in this study. Of the offspring, eleven grew to adult form, exhibiting a range of Nps-1 through Nps-4 morphologies. Of importance is that one of the offspring underwent gametogenesis and was therefore a gamont. However, it is unlikely that the dextral offspring in this study were also gamonts, since no dextral specimens have ever been observed to release gametes and the Medium proloculus (gamont) sizes are absent in the dextral assemblage in this study (Fig. 7A). One possible explanation for this surprising outcome is the observation in benthic foraminifera that meiosis occasionally fails during multiple fission in culture. Under this scenario, offspring could be a mix of both schizonts and gamonts (Le Calvez, 1946), which might explain the unusual coiling ratio for *N. pachyderma* observed in the Davis et al. (2020) culture. Furthermore, there is a wide scatter around the mean proloculus size for the Small dextral proloculus group in our study (Fig. 7A). The lower proloculus values described in Davis et al. (2020) would fall well within it, supporting our suggestion that some of the observed offspring could be schizonts.

Previous studies therefore suggest we might expect schizonts in successive clonal generations (Meilland et al., 2024), and potentially following failed meiosis, when both schizonts and gamonts can be produced (Le Calvez, 1946); but the mechanism determining the coiling ratio in schizonts remains unknown. For example, in the benthic foraminifera *Amphistegina* spp., schizonts and gamonts show a predominant coiling direction, while agamonts may not (Hallock and Larsen, 1979). It is clear that the agamonts can be either sinistral or dextral coiling (Darling et al., 2023), but it is unknown whether the schizont clones exhibit the coiling direction of the parent test when they clone themselves. If they did, it could account for the unusually high level of dextral coiling in the Small proloculus fraction observed in this study. At present, no definitive mechanism has been proposed to explain these coiling patterns in *N. pachyderma* and other species, and this question remains open.

Meilland et al. (2024) recorded the proloculus sizes and coiling direction of seven initial parent tests whose offspring went on to produce a second generation of offspring. Although the Meilland et al. (2024) study was an enormous undertaking, with 29 reproductive events that produced about 33,000 offspring, the numbers of actual offspring successfully measured for both proloculus size and coiling direction per reproduction was relatively limited. The proloculus sizes of the initial parent tests varied widely, with three specimens (two sinistral and one dextral coiling) exhibiting a small proloculus (12.6 μm , 14.59 μm , and

7.5 μm). These sizes are all defined in Meiland et al. (2022) as microspheric. The specimen with the 12.6 μm proloculus, for example, produced two further generations of offspring with a similar small size proloculus to those in this study. These are most likely to be successive clonal reproductive events since all generations have a small proloculus. However, the variation in parent proloculus sizes in the seven initial parent tests suggests that they may have been a mixture of agamonts and schizonts at various stages of transition between the two states. To terminate the schizont cycle, meiosis and multiple fission must be triggered in a schizont to produce gamont offspring again. It remains unknown what triggers the clonal cycle to commence, or what determines the number of schizont cycles.

4.2.3. Environmental influence on *N. pachyderma*'s reproduction cycle in the CAO

We hypothesise that the *N. pachyderma* assemblage in the CAO water column is dominated and sustained by an asexual schizont cycle (Fig. 8), which is reflected in the high abundance of Small proloculi individuals in both the Nps-5 and Npd populations. This cycle allows rapid population expansion, particularly in extreme environments like the CAO, where successive asexual generations may sustain populations under resource-limited conditions. This suggests that the ambient conditions (Vermassen et al., 2025), together with low or even the absence of light under the thick perennial sea ice, influences the reproductive strategy of *N. pachyderma* in the CAO.

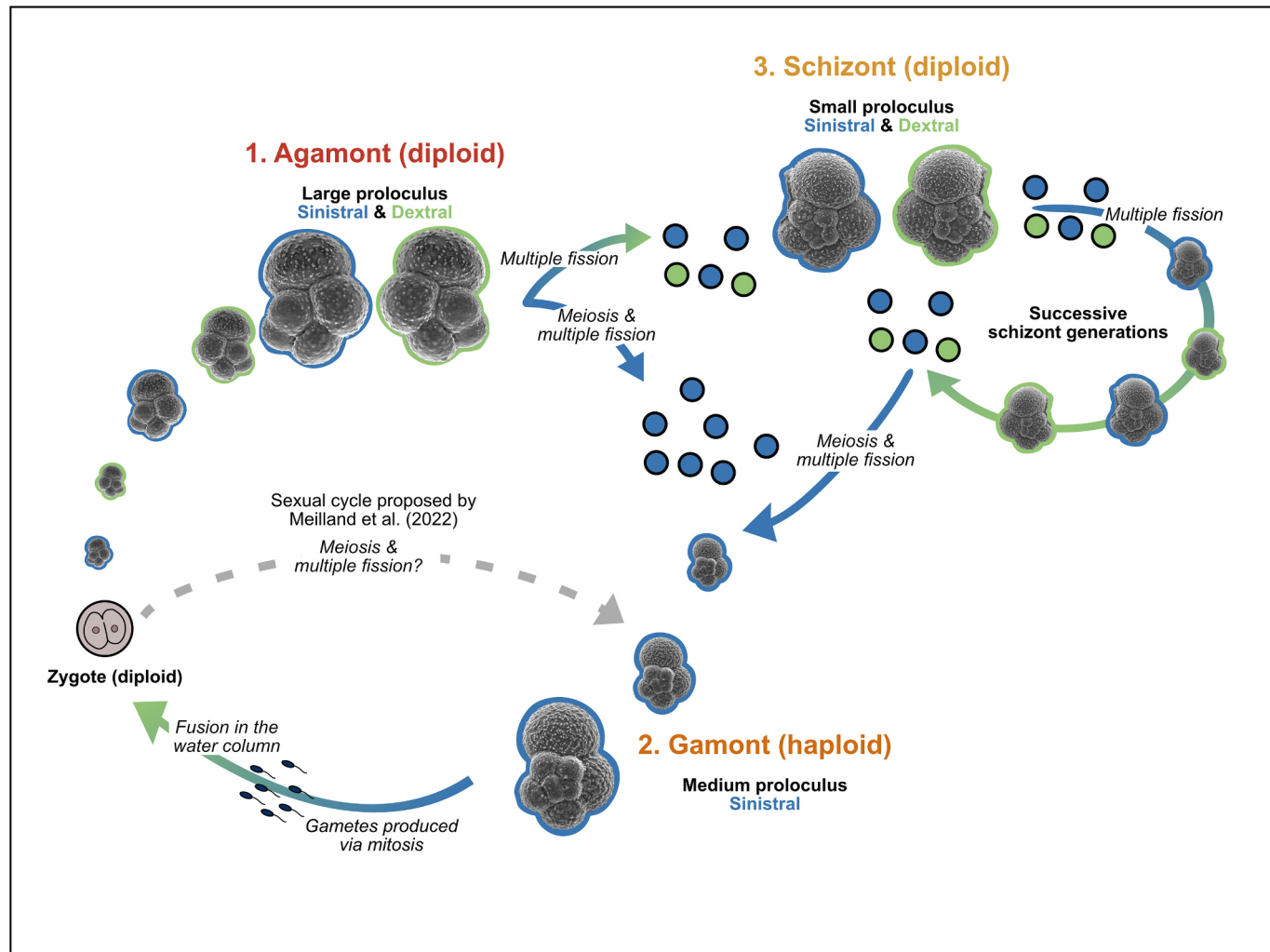


Fig. 8. Proposed trimorphic life cycle of *Neogloboquadrina pachyderma*, modified from Darling et al. (2023) and Dettmering et al. (1998), incorporating proloculus sizes for the gamont (orange; Medium proloculus), agamont (red; Large proloculus), and schizont (yellow; Small proloculus), based on the GMM dataset (Table 2). The life cycle is derived from a combination of both benthic and non-spinose planktonic foraminiferal literature, consistent with the position of meiosis within the benthic foraminiferal clades (Goldstein, 2002; Goetz et al., 2022). Dextral individuals (green) and sinistral individuals (blue) are indicated. In the primary cycle, diploid zygotes develop into large proloculus agamonts (red) which may coil in both directions. They produce high numbers of gamonts (orange) through meiosis and multiple fission. These represent the typical *N. pachyderma* sinistral population of the water column. The haploid gamonts then release gametes that fuse to form a diploid zygote, to complete the primary dimorphic cycle. Diploid agamont (red; Large proloculus) may also reproduce asexually by cloning to produce diploid small-proloculus schizonts (yellow). Schizonts can either reproduce asexually via schizogony giving rise to successive schizont generations, or undergo meiosis and multiple fission giving rise to Medium proloculus gamonts. These in turn release haploid gametes into the water column which fuse to form zygotes, thus closing the cycle. While we acknowledge the solely sexual cycle as proposed by Meiland et al. (2022) is possible, we emphasise that an exclusively sexual cycle has not been observed in benthic foraminifera from which the planktonic foraminifera originated. The sexual cycle follows Meiland et al. (2022), however, the position of meiosis and multiple fission in this cycle is unknown. The asexual cycle aligns with observations from Darling et al. (2023) and Meiland et al. (2022, 2024). A hypothesised schizont cycle, based on Darling et al. (2023) and Meiland et al. (2024), suggests that successive schizogony prolongs asexual reproduction, maintaining population stability under Arctic conditions. The three reproductive modes (sexual gamont, asexual agamont, and asexual schizont) are illustrated with representative SEM images of specimens with Small, Medium, and Large proloculi, corresponding to the schizont, gamont, and agamont stages, respectively. (For interpretation of the references to colour in this figure legend, the reader is referred to the web version of this article.)

Although the exact mechanisms remain unclear, one possibility is that epigenetic processes may play a role in regulating reproduction modes under environmental stress. [Hallock and Reymond \(2022\)](#) suggest that the release of schizonts in larger benthic foraminifera may represent an epigenetically-induced stress response by the parent, where changes in gene function can be inherited across generations without altering DNA sequences and may gradually reverse when stress conditions ease ([Parker et al., 2022](#)). Protists, including foraminifera, have been shown to possess potential for epigenetic regulation ([Weiner et al., 2020](#)), but further research is needed to determine if such mechanisms are involved in *N. pachyderma*'s reproduction cycle in the CAO.

The ecology and depth habitat of *N. pachyderma* in the CAO is likely shaped by light availability and light-dependent processes, particularly in relation to sea ice cover and chl-*a* concentrations ([Greco et al., 2019](#)). During the SAS-Oden 2021 cruise, the average sea ice thickness at our stations was 1.77 m (max. 2.6 m), with an average snow cover of around 3 cm ([Snoeijis-Leijonmalm and the SAS-Oden Scientific Party, 2022](#)). Given these conditions, light transmittance through the sea ice at the time of the cruise was likely very low, as previous studies have shown that light transmission decreases with both increased ice thickness and overlying snow cover. For example, a 10 cm snow layer can reduce light transmittance to below 5 % ([Perovich, 2007](#); [Nicolaus et al., 2013](#); [Perovich, 2017](#)), meaning that light transmittance during the SAS-Oden 2021 cruise was low. The possibility of a light-limiting effect on *N. pachyderma* reproduction could be supported by the unusual high dextral coiling assemblage (35 %) observed in *N. pachyderma* cultures following 24-h darkness treatment ([Davis et al., 2020](#)), though this requires further investigation. If the Npd assemblage with Small proloculi in the CAO reflects a schizont cycle, its abundance may be a consequence of the unique conditions associated with perennial sea-ice cover, specifically, reduced light levels due to thicker sea ice and snow cover. This suggestion is strongly supported by the consistently low dextral coiling values (<3 %) observed further south in the high latitude polar North Atlantic, where summer sea ice is absent ([Bauch et al., 2003](#); [Darling et al., 2006](#)).

4.2.4. Reproductive timing of *N. pachyderma* in the CAO

While we recognise the potential for a solely sexual cycle in the high latitudes as suggested by [Meilland et al. \(2022\)](#) (indicated by the grey arrow in [Fig. 8](#)), our data suggests a more complex scenario in the CAO, where gamonts may arise from both agamonts and schizonts. The strictly sexual cycle, suggested by [Hemleben et al. \(1989\)](#) for the planktonic foraminifera remains unobserved in benthic foraminifera ([Darling et al., 2023](#)), from which the planktonic foraminifera evolved. Given that different modern planktonic foraminiferal groups may have evolved independently from their benthic ancestors ([Darling et al., 1997](#); [Morard et al., 2024](#)) and acquired new traits, we acknowledge the possibility of a sexual cycle for members of the non-spinose planktonic foraminiferal group in our reproduction model.

We recognise the contributions of [Meilland et al. \(2022\)](#) and these insights are part of an evolving understanding, particularly considering that their results are based on culture studies, while our findings are grounded in field data under the most extreme of polar conditions (i.e. perennial sea ice cover). This difference underscores the need for further research, as we do not yet have enough clarity to construct a definitive picture of *N. pachyderma*'s reproductive cycle. Following [Darling et al. \(2023\)](#), we therefore hypothesise that the exceptionally large proportion of aberrant coilers that we observe are most likely the result of a clonal schizont cycle, involving successive asexually produced generations that rapidly build up standing stock in the seasonally extreme CAO environment. This mode of reproduction, recognised for the first time in the field on our Arctic SAS-2021 expedition, is a well-known phenomenon in benthic foraminifera (e.g., [Leutenegger, 1977](#); [Dettmering et al., 1998](#); [Goldstein, 2002](#)), and has only been reported recently for the non-spinose planktonic group in culture ([Meilland et al., 2024](#)).

The unique environmental setting of the CAO is highlighted when

comparing sediment trap data from the subarctic North Pacific. Here the sediment traps reveal two distinct flux peaks of *N. pachyderma*, each lasting 30–40 days and approximately equal in magnitude ([Sautter and Thunell, 1989](#); [Alderman, 1996](#)), coinciding with a spring and autumn phytoplankton bloom ([Sigler et al., 2014](#)). Dextral coiling in this region never exceeds 3 % ([Alderman, 1996](#)), suggesting dominance of the typical agamont–gamont sexual cycle. In contrast, the CAO exhibits a single, summer phytoplankton bloom which is initiated when sea ice cover is still intense and up to 2 m thick ([Ko et al., 2024](#)), highlighting the region's unique environmental constraints and the specific adaptations of its planktonic communities.

Across the Sub-Arctic and Arctic, phytoplankton blooms vary in timing and intensity. The earliest blooms occur in the Nordic and Bering seas, while one of the latest is recorded in the CAO ([Ardyna et al., 2013](#)). This summer bloom is influenced by the relatively short growing season due to the persistent sea ice cover. In multi-year ice-covered regions in the CAO, conditions typically support only one broad bloom ([Ko et al., 2024](#)), which may be muted or subsurface due to the ice cover that prevent wind-driven vertical mixing and nutrient replenishment of the surface layer ([Ardyna et al., 2014](#)). Light availability is a key limiting factor in the Arctic, where the typical 24-h diurnal cycle is replaced by extended periods of continuous daylight during summer (midnight sun) and prolonged darkness during winter (polar night), resulting in pronounced seasonal variations that affect biological and reproductive processes differently throughout the year.

In the CAO, the under-ice phytoplankton bloom initiates between late May and late June peaking in early August ([Ko et al., 2024](#)). We speculate that the single bloom, and thus short time window for feeding, likely influences the reproduction mode of *N. pachyderma*. During the onset of the phytoplankton bloom, overwintering schizonts likely graze on the phytoplankton to build energy reserves for reproduction. Schizonts may be better suited for overwintering than gamonts, as culture studies have shown schizont offspring survival over six months of dormancy ([Meilland et al., 2024](#)). These dormant schizonts may resume activity when stimulated by food availability, as was suggested for some benthic species (e.g. [Myers, 1942](#); [DeLaca et al., 1980](#)). Once favourable conditions return during spring with increasing sunlight and sea ice biomass in the CAO ([Harney et al., 1998](#)), schizonts would be stimulated out of dormancy by food availability and are likely to enter meiosis and multiple fission to produce gamonts, thereby initiating the agamont–gamont reproductive cycle, rather than continuing with clonal reproduction.

In addition to the potential for dormancy in overwintering schizont population, studies of living planktonic foraminifera during the polar night in the Barents Sea indicate that *N. pachyderma* could survive the harsh conditions of winter sea-ice cover, feeding on a wide variety of food ([Zamelczyk et al., 2021](#)). *Neogloboquadrina pachyderma* from Baffin Bay feed predominantly on diatoms, Crustacea and bacteria ([Greco et al., 2021a](#); [Bird et al., 2024, in review](#)). Brine pockets in sea ice can store viable diatoms with intact chloroplasts in winter months which are then released into the under-ice waters upon melting the following spring ([Krembs et al., 2002](#)). [Zamelczyk et al. \(2021\)](#) found that planktonic foraminifera were present in low abundances in the upper 50 m during the Arctic polar night, evidencing survival under harsh winter conditions. Benthic foraminifera have also been shown to remain metabolically active during the polar night and seem to have access to algal food ([Knyazeva and Korsun, 2016](#)). This indicates that, although *N. pachyderma* standing stock may decrease by a factor of >200 during winter ([Vilks, 1989](#)), it has the ability to overwinter, potentially as schizonts, by feeding when active on food released from the sea ice. This surviving schizont population would serve as the starting standing stock for the upcoming season. However, unlike Antarctic *N. pachyderma* Type IVa, which has been observed living in sea ice brine channels ([Spindler and Dieckmann, 1986](#)), the Arctic *N. pachyderma* Type Ia does not appear to be adapted to this habitat, as no living or dead foraminifera were found in Arctic sea ice ([Gradinger, 1999](#)).

We speculate that under favourable summer conditions, when nutrient levels are high, these schizonts give rise to gamonts, thereby initiating the sexual cycle. By July, the water column likely contain relatively few schizonts, each producing large numbers of gamonts. As the bloom progresses and reaches its peak in early August, the proportion of dextral individuals increases, reaching a maximum by late August to early September (Fig. 3). This pattern suggests that, in addition to the regular agamont-gamont cycle, successive rounds of schizont reproduction are also occurring. These coincide with declining Chl. *a* concentrations, indicating the initiation of bloom termination and conditions less favourable for sexual reproduction. Under these circumstances, the energetically less demanding schizont cycle (e.g. Crow, 1994) may be favoured, potentially continuing until phytoplankton bloom termination in mid-October (Ko et al., 2024).

Additionally, Stations 1–4 show the smallest average test areas for Nps-5 and Npd among all stations (ca. $0.96 \times 10^4 \mu\text{m}^2$ and $1.05 \times 10^4 \mu\text{m}^2$, respectively; Fig. 4 and Supplementary Table 8), suggesting these populations are likely the youngest and represent the onset of the schizont cycle. In contrast, Stations 5 and 6 exhibit slightly larger test areas for Nps-5 and Npd ($1.07 \times 10^4 \mu\text{m}^2$ and $1.1 \times 10^4 \mu\text{m}^2$, respectively; Fig. 4 and Supplementary Table 8) along with a higher abundance of dextral coilers compared to Stations 1–4, indicating that more successive clonal reproduction events have already occurred at these two sites.

Therefore, the limited duration of the phytoplankton bloom in the CAO constrains the schizont cycle to a narrow window as is evidenced by the mismatch between the dextral coiling percentages in the water column (up to 32 %) and lower values in the underlying sediment (ca. 6 %). Given the background dextral signature of <3 % from the agamont-gamont cycle, the sedimentary signal reflects a brief yet substantial contribution from schizont-driven reproduction. Despite being muted by the dominantly sinistral agamont-gamont cycle, the elevated sedimentary dextral ratio confirms the impact of the seasonal schizont cycle in the CAO.

The co-occurrence of gamonts, agamonts, and schizonts during summer suggests that all three reproductive modes operate simultaneously in the CAO, likely as a regional adaptation to sea ice and bloom timing. One exception is Station 8 (Yermak Plateau), which recorded the lowest dextral abundance and few *T. quinqueloba* specimens. Its peripheral location to the CAO suggests greater influence from Greenland and Barents Seas hydrography and phytoplankton bloom dynamics, differing from CAO conditions. This influence is consistent with North Atlantic Water advection into subsurface layers, as shown by Hillaire-Marcel et al. (2004), who documented distinct $\delta^{18}\text{O}$ signatures across different size fractions of *N. pachyderma* from the Chukchi Sea and Northwest Atlantic sediments, reflecting water mass mixing and advection processes in the Central Arctic Ocean. The sea ice minimum recorded near Station 8 on September 10th 2021 (Vermassen et al., 2025) likely influenced local dynamics, potentially affecting the sinistral:dextral abundance when compared to the other stations. One possibility is that schizont reproduction had commenced earlier, as indicated by the larger Npd and Nps-5 test area sizes ($\sim 1.4 \times 10^4 \mu\text{m}^2$; Fig. 4 and Supplementary Table 8) and 8.8 % dextral coiling. On the other hand, due to the region's transitional hydrographic setting i.e. intermediate between the CAO and the Nordic Seas, the reproductive season including gamonts, agamonts, and schizonts may be extended in this region. This could result in a more gradual build-up of schizonts over time, rather than the sharp peak seen in the CAO. Therefore, when sampled, Station 8 may have been at an earlier stage of its own schizont succession, even if schizont reproduction had started earlier than in the CAO. In this scenario, we are suggesting a slower progression and potentially lower peak abundance in schizonts due to milder environmental conditions. Neither can be excluded at this stage.

Together, these observations support incorporating the schizont cycle into the reproductive framework of *N. pachyderma* as an adaptation to the CAO's extreme, perennially sea-ice covered environment.

High numbers of both dextral and sinistral schizonts with small proloculi suggest that successive schizont generations sustain populations when the seasonal time window for sexual reproduction is too short to support multiple gamont-agamont reproductive cycles. This reproductive flexibility would reinforce *N. pachyderma*'s ability to persist in resource-limited environments, such as under perennial sea ice, where successive clonal schizont reproduction would enhance population stability and survival.

4.3. Mismatch between dextral coilers in the water column versus surface sediments

A further key observation in our Central Arctic studies is the higher proportions of dextral coiling specimens in the central Arctic water column compared to underlying sediments, which in this study range between 5.3 % to 6.2 % (Supplementary Table 3). These water column specimens are also generally smaller in size than their sediment counterparts (Fig. 4), suggesting they represent an earlier life stage or an active reproductive phase. Additionally, the discrepancy may partly reflect a proportion of *N. pachyderma* specimens failing to grow and develop to maturity (Meilland et al., 2022), making them more susceptible to dissolution in the water column and sediment due to their thin tests. Immature tests are thin walled (Plate 3) and only a proportion of both dextral and sinistral coiling specimens are likely to reach maturity to reproduce in the challenging environment of the CAO. Prior to reproduction, mature sinistral gamonts are known to thicken their tests prior to gamete release, which makes them much more resistant to dissolution in the water column and sediment (Plate 2, Figs. 16, 17). However, it is unknown how resistant mature schizont tests are to dissolution. Although Npd tests exhibited a similar scale of morphological variability to sinistral morphotypes (Plate 1, Figs. 15–19 and Plate 2, Figs. 16–20), schizonts may not necessarily produce a secondary calcite layer prior to offspring release. Meilland et al. (2024) report that all the agamonts and schizont parent tests that reproduced in culture by multiple fission had thin translucent tests. However, the agamonts with the Large proloculus do persist in the sediments, since they represent the <3 % dextral coiling specimens observed throughout the fossil assemblages, except for the CAO. Whether the slightly elevated dextral percentages observed in the CAO core tops persist downcore may address this dissolution question.

The production of schizonts may also be seasonal as we speculate, though always produced in parallel with sinistral gamont production, since the gamonts constitute a substantial component of the CAO water column assemblages in this study. The timing of the SAS-Oden 2021 sampling might therefore have coincided with an asexual schizont reproduction event, increasing the dextral coiling signature of the assemblage at the time of sampling.

Although there is a large mismatch between the water column proportions of dextrally coiled *N. pachyderma* and the expected maximum 3 % aberrant coiling paradigm (Darling et al., 2006), as well as between the abundance of dextral coilers in the water column compared to the seafloor, most seafloor samples in this study also show marginally higher aberrant coiling than the 3 % paradigm (Darling et al., 2006). This is not a unique observation for the CAO, with various studies reporting deviations in different Arctic regions. Dextral coiling specimens are recorded at frequencies of ca. 4 % in the Canadian Arctic Archipelago ($>63 \mu\text{m}$ fraction) (El Bani Altuna et al., 2018), 2–7 % in the Siberian and Central Arctic Ocean ($>150 \mu\text{m}$ fraction, there referred to as *N. incompta*; Prabhakar et al., 2024) and 3.1–9.1 % from the Central Lomonosov Ridge/Amundsen Basin ($>63 \mu\text{m}$ fraction; Nørgaard-Pedersen et al., 2007). The sediment relative abundances of dextral-coilers from our SAS-Oden 2021 study falls within the range of these reported literature values, where average sediment dextral coiling is 5.8 %, reaching a maximum of 6.2 % at Station 1 (Supplementary Table 6). The extent to which this signal persists in downcore CAO sediments remains unknown. We propose that this deviation from the 3 % aberrant coiling

paradigm (Darling et al., 2006) in the CAO sediments represents the signature of regional schizont production, which may be unique to the central Arctic waters.

A key difference between our water column populations and sediment samples is the higher abundance of immature specimens in the water column, evidenced by the large proportion of Npd and Nps-5 and their smaller size (Fig. 4, Supplementary Table 8). In contrast, the sediments are characterised with the higher abundance of more mature forms (Nps-1 through Nps-4). This water column-sediment mismatch was also identified in the Northeast Water Polynya, offshore north-eastern Greenland (Kohfeld et al., 1996). The mismatch is likely due to the plankton nets capturing a seasonal snapshot with multiple life stages, in contrast with surface sediments that preserve death assemblages dominated by mature individuals averaged over years to decades.

4.4. Palaeoceanographic significance of *N. pachyderma* morphotypes including aberrant coilers

Beyond the need to distinguish *N. pachyderma* dextral (Npd) from *N. incompta*, critical to avoiding erroneous warm-water signals, understanding the habitat and calcification depth of *N. pachyderma* in ice-covered regions is also essential for other types of palaeoceanographic analysis, particularly geochemical reconstructions of stratified water-masses (e.g. $\delta^{18}\text{O}$, $\delta^{13}\text{C}$, $\delta^{15}\text{N}$) (Xiao et al., 2014; Farmer et al., 2021). Our plankton distributions can provide useful insights in this context. Previous studies have speculated that the different *N. pachyderma* morphotypes reflect different ecologies or depth habitats potentially adding nuance to Arctic geochemical reconstructions (e.g. Hillaire-Marcel et al., 2004). The few existing $\delta^{18}\text{O}$ and $\delta^{13}\text{C}$ studies involving multi-morphotype $\delta^{18}\text{O}$ and $\delta^{13}\text{C}$ separations, however, produce diverging results. For example, $\delta^{18}\text{O}$ and $\delta^{13}\text{C}$ measured on sedimented *N. pachyderma* by El Bani Altuna et al. (2018) suggested that Nps-5 indicated deeper surface waters compared to Nps-1 through Nps-4. In contrast, Prabhakar et al. (2024) found little difference in isotopic measurements between the morphotypes, including Nps-5 (their Nps-3), suggesting that separating morphotypes may not be necessary for $\delta^{18}\text{O}$ and $\delta^{13}\text{C}$ analyses. Our own water column morphotype distributions support this latter view: we observe no clear depth differentiation for Nps-1 through Nps-4, which are the heavily encrusted forms most common in the sediment. Instead, our data suggest the gametogenic calcite forming these morphotypes is generally added below 200 m depth (Fig. 2). Stable isotope analyses on the plankton tow specimens are beyond the scope of this work, but would be essential to further clarifying these patterns.

The (mis)identification of *N. incompta* in the CAO has already occurred in the literature. Prabhakar et al. (2024) referred to the dextral coiling morphotype recorded in their samples from the central and Siberian Arctic as *N. incompta*, on the grounds that their sediment-sample dextral:sinistral coiling ratio exceeds the 3 % aberrant coiling *N. pachyderma* threshold, although no actual count data is presented in the study. We are not convinced this is true *N. incompta* and suggest it may instead be dextral coiling *N. pachyderma*, based on the observations made in this study. *Neogloboquadrina incompta* is well documented as being confined to the subpolar transitional waters between polar and temperate zones in the North Atlantic (e.g. Greco et al., 2021b). Although Atlantification is progressing northward (e.g., Polyakov et al., 2017; Ingvaldsen et al., 2021), *N. incompta* is highly unlikely to be present in the CAO water column at temperatures as low as $-1.5\text{ }^{\circ}\text{C}$ (Vermassen et al., 2025), either today or anytime during the Holocene (Siccha and Kucera, 2017). While *N. incompta* has been recorded in the southern Barents Sea over the past three millennia, it remains virtually absent from the northern Barents Sea, highlighting a persistent biogeographic boundary between the high latitude North Atlantic and the CAO (Anglada-Ortiz et al., 2025). In subpolar assemblages, *N. incompta* would also be accompanied by significant proportions of the other subpolar species such as, *Globigerina bulloides* (e.g. Greco et al.,

2021b), which is not reported in Prabhakar et al. (2024), and *T. quinqueloba* (e.g. Ofstad et al., 2021). All genotyping of *N. pachyderma* (including Central Arctic *N. pachyderma* and coiling specimens) in both the Central Arctic (this study) and the Fram Strait (Bauch et al., 2003) has revealed a single genotype, *N. pachyderma*: Type 1a (Darling et al., 2006, this study).

5. Conclusion

Our study is a comprehensive analysis of *N. pachyderma* in the central Arctic Ocean, focusing on its vertical distribution, morphotypes, size classes, and reproductive strategies under perennial sea-ice conditions. The findings of this study offer a deeper understanding of planktonic foraminifera dynamics in ice-covered regions and their implications for interpreting sediment records and climate reconstructions.

We observed that *N. pachyderma* dextral, considered rare ($<3\text{ }\%$) in the water columns and sediments worldwide (Darling et al., 2006), were found at significantly higher proportions (up to $32.3\text{ }\%$) in the CAO water column. The dextral coilers are not *N. incompta* and we propose that they are asexually produced clonal schizonts, as demonstrated in *N. pachyderma* cultures of Meiland et al. (2024), since all genotyped specimens in this study were identified as *N. pachyderma*. These findings support the hypothesis that *N. pachyderma* has a complex three component life cycle: a sexual gamont stage (Medium proloculus), an asexual agamont stage (Large proloculus), and a secondary asexual stage producing schizonts (Small proloculus). The high abundance of dextral coiling *N. pachyderma* with a Small proloculus are interpreted as being an indicator of an active asexual clonal schizont cycle that occurred in parallel with the typical sexual/sexual cycle, based on proloculus size distributions from both previous culture studies and our new observations in the CAO.

We propose that this reproductive strategy is an adaptation to extreme Arctic conditions, particularly under intense sea ice cover at the time of sampling. The longevity of schizonts and their capacity for rapid clonal reproduction would allow *N. pachyderma* Type 1a to quickly expand its population following winter dormancy, taking advantage of the brief summer bloom in the high Arctic. We suggest that schizonts initially produce gamonts during the early and median stages of the phytoplankton bloom, when food is abundant. As the bloom intensity decreases and environmental conditions become less favourable, *N. pachyderma* initiates the schizont cycle, alongside the agamont-gamont cycle. This late season schizont cycle increases the population standing stock ahead of winter, enhancing *N. pachyderma*'s overwinter survival under ice-covered, nutrient-limited conditions. The much lower abundance of dextral coilers in the underlying sediments (average $5.8\text{ }\%$ across all stations) highlights that asexual schizont reproduction is a proportionately rare event associated with the late summer bloom.

From a palaeoceanographic perspective, misidentifying an elevated abundance of *N. pachyderma* dextral morphotypes as *N. incompta* could lead to erroneous palaeoclimate interpretations. While we do not rule out the potential of *N. incompta*, accompanied by other subpolar planktonic foraminifera, to invade the CAO in the future due to Atlantification and Arctic warming, we believe the dextral forms in this study are *N. pachyderma*. The high prevalence of dextral individuals in the CAO water column and raised dextral values in the CAO sediments challenges the $<3\text{ }\%$ paradigm being applied to the Arctic polar waters. This perspective should be considered before assigning dextrally coiled specimens to *N. incompta* in these regions.

CRediT authorship contribution statement

Tirza M. Weitkamp: Writing – original draft, Visualization, Methodology, Investigation, Formal analysis, Data curation, Conceptualization. **Clare Bird:** Writing – review & editing, Resources, Investigation, Formal analysis, Data curation, Conceptualization. **Kate F. Darling:** Writing – review & editing, Conceptualization. **Allison Y. Hsiang:**

Writing – review & editing, Software, Formal analysis, Conceptualization. **Jemma Ramsay:** Investigation. **Flor Vermassen:** Writing – review & editing, Resources, Investigation. **Helen K. Coxall:** Writing – review & editing, Supervision, Funding acquisition, Conceptualization.

Funding sources

This research has been supported by Swedish Research (VR) grant no. DNR 2019–03757 and grant no. DNR 2023–03792 awarded to Helen K. Coxall.

Declaration of competing interest

The authors declare that they have no known competing financial interests or personal relationships that could have appeared to influence the work reported in this paper.

Acknowledgements

This research is dependent on samples collected by ice breaker Oden, a key item of Swedish Research Council-funded national infrastructure. We are grateful to the captain and crew of IB Oden for their skilful operation of the vessel during the expedition. The Swedish Polar Research Secretariat (SPRS) provided valuable support with scientific equipment and expedition logistics. The scientific leadership of the SAS ODEN21 expedition (Pauline Snoeijis-Leijonmalm) is acknowledged for planning and coordination. This research has been supported by Swedish Research Council (VR) grant no. DNR 2019–03757 and grant no. DNR 2023–03792 awarded to Helen K. Coxall. We also thank the two anonymous reviewers for their comments and suggestions, which greatly helped improve the manuscript.

Appendix A. Supplementary data

Supplementary data to this article can be found online at <https://doi.org/10.1016/j.marmicro.2025.102503>.

Data availability

The data that support the findings of this study are openly available in the Bolin Centre Database at <https://doi.org/10.17043/oden-sas-2021-foraminifera-morphometric-1>

References

- Alderman, S.E., 1996. Planktonic Foraminifera in the Sea of Okhotsk: Population and Stable Isotopic Analysis from a Sediment Trap. M.Sc. MIT/WHOI, Cambridge, MS, p. 99.
- Anglada-Ortiz, G., Zamelczyk, K., Meiland, J., Ziveri, P., Chierici, M., Fransson, A., Rasmussen, T.L., 2021. Planktic Foraminiferal and Pteropod Contributions to Carbon Dynamics in the Arctic Ocean (North Svalbard margin). *Front. Mar. Sci.* 8. <https://doi.org/10.3389/fmars.2021.661158>.
- Anglada-Ortiz, G., Rasmussen, T.L., Chierici, M., Fransson, A., Ziveri, P., Thomsen, E., Zamelczyk, K., Meiland, J., Ezat, M.M., Garcia-Orellana, J., 2025. Changes in Planktic Foraminiferal distribution, Productivity, and Preservation in the Barents Sea during the last three Millennia. *Paleoceanography and Paleoclimatology* 40 (4). <https://doi.org/10.1029/2024PA004989> e2024PA004989.
- Ardyna, M., Babin, M., Gosselin, M., Devred, E., Bélanger, S., Matsuoka, A., Tremblay, J.-É., 2013. Parameterization of vertical chlorophyll in the Arctic Ocean: Impact of the subsurface chlorophyll maximum on regional, seasonal, and annual primary production estimates. *Biogeosciences* 10 (6), 4383–4404. <https://doi.org/10.5194/bg-10-4383-2013>.
- Ardyna, M., Babin, M., Gosselin, M., Devred, E., Rainville, L., Tremblay, J.-É., 2014. Recent Arctic Ocean sea ice loss triggers novel fall phytoplankton blooms. *Geophys. Res. Lett.* 41 (17), 6207–6212. <https://doi.org/10.1002/2014GL061047>.
- Arnold, Z.M., 1955. Life history and cytology of the foraminiferan *Allogromia laticollaris*. *Univ. Calif. Publ. Zool.* 61, 167–252.
- Backman, J., Jakobsson, M., Lovlie, R., Polyak, L., Febo, L.A., 2004. Is the Central Arctic Ocean a sediment starved basin? *Quat. Sci. Rev.* 23 (11), 1435–1454. <https://doi.org/10.1016/j.quascirev.2003.12.005>.
- Bandy, O.L., 1960. The geologic significance of coiling ratios in the foraminifer *Globigerina pachyderma* (Ehrenberg) [California]. *J. Paleo.* 34 (4), 671–681.
- Bauch, D., Darling, K., Simstich, J., Bauch, H.A., Erlenkeuser, H., Kroon, D., 2003. Palaeoceanographic implications of genetic variation in living North Atlantic *Neogloboquadrina pachyderma*. *Nature* 424 (6946), 299–302. <https://doi.org/10.1038/nature01778>.
- Bird, C., Darling, K.F., Thiessen, R., Pieńkowski, A.J., 2024. The 16S rRNA microbiome of the Arctic foraminifera *Neogloboquadrina pachyderma* comprised of hydrocarbon-degrading bacteria and a diatom chloroplast store. *EGUphere* 1–48. <https://doi.org/10.5194/egusphere-2024-497>.
- Brummer, G.-J.A., Hemleben, C., Spindler, M., 1987. Ontogeny of extant spinose planktonic foraminifera (Globigerinidae): a concept exemplified by *Globigerinoides sacculifer* (Brady) and *G. ruber* (d'Orbigny). *Mar. Micropaleontol.* 12, 357–381. [https://doi.org/10.1016/0377-8398\(87\)90028-4](https://doi.org/10.1016/0377-8398(87)90028-4).
- Carstens, J., Wefer, G., 1992. Recent distribution of planktonic foraminifera in the Nansen Basin, Arctic Ocean. *Deep-Sea Res. I Oceanogr. Res. Pap.* 39 (2), S507–S524.
- Chassagnol, B., Bichat, A., Boudjeniba, C., Wuillemin, P.-H., Guedj, M., Gohel, D., Nuel, G., Becht, E., 2023. Gaussian Mixture Models in *R*. *R J.* 15 (2), 56–76.
- Crow, J.F., 1994. Advantages of sexual reproduction. *Dev. Genet.* 15 (3), 205–213. <https://doi.org/10.1002/dvg.1020150303>.
- Darling, K.F., Wade, C.M., Kroon, D., Brown, A.J.L., 1997. Planktic foraminiferal molecular evolution and their polyphyletic origins from benthic taxa. *Mar. Micropaleontol.* 30, 251–266.
- Darling, K.F., Kucera, M., Pudsey, C.J., Wade, C.M., 2004. Molecular evidence links cryptic diversification in polar planktonic protists to Quaternary climate dynamics. *PNAS* 101 (20), 7657–7662. <https://doi.org/10.1073/pnas.0402401101>.
- Darling, K.F., Kucera, M., Kroon, D., Wade, C.M., 2006. A resolution for the coiling direction paradox in *Neogloboquadrina pachyderma*: coiling direction in *N. pachyderma*. *Paleoceanogr.* 21 (2). <https://doi.org/10.1029/2005PA001189>.
- Darling, K.F., Husum, K., Fenton, I.S., 2023. The biphasic life cycle of the non-spinose planktonic foraminifera is characterised by an aberrant coiling signature. *Mar. Micropaleontol.* 185, 1–10. <https://doi.org/10.1016/j.marmicro.2023.102295>.
- Davis, C.V., Livsey, C.M., Palmer, H.M., Hull, P.M., Thomas, E., Hill, T.M., Benitez-Nelson, C.R., 2020. Extensive morphological variability in asexually produced planktic foraminifera. *Sci. Adv.* 6 (28). <https://doi.org/10.1126/sciadv.abb8930>.
- DeLaca, T.E., Lipps, J.H., Hessler, R., 1980. The morphology and ecology of a new large agglutinated Antarctic foraminifer (*Textulariina: Notodendrodidae nov.*). *Zool. J. Linn. Soc.* 69 (3), 205–224.
- Dettmering, C., Röttger, R., Hohenegger, J., Schmaljohann, R., 1998. The trimorphic life cycle in foraminifera: Observations from cultures allow new evaluation. *Eur. J. Protistol.* 34 (4), 363–368. [https://doi.org/10.1016/S0932-4739\(98\)80004-7](https://doi.org/10.1016/S0932-4739(98)80004-7).
- Duan, B., Li, T., Pearson, P.N., 2021. Three dimensional analysis of ontogenetic variation in fossil globorotaliiform planktic foraminiferal tests and its implications for ecology, life processes and functional morphology. *Mar. Micropaleontol.* 165, 1–9. <https://doi.org/10.1016/j.marmicro.2021.101989>.
- El Bani Altuna, N., Pieńkowski, A.J., Eynaud, F., Thiessen, R., 2018. The morphotypes of *Neogloboquadrina pachyderma*: Isotopic signature and distribution patterns in the Canadian Arctic Archipelago and adjacent regions. *Mar. Micropaleontol.* 142, 13–24. <https://doi.org/10.1016/j.marmicro.2018.05.004>.
- Ericson, D.B., 1959. Coiling direction of *Globigerina pachyderma* as a climatic index. *Science* 130 (3369), 219–220.
- Eynaud, F. (2011). Planktonic foraminifera in the Arctic: potentials and issues regarding modern and quaternary populations. In *IOP Conference Series: Earth and Environmental Science* (Vol. 14, No. 1, p. 012005). IOP Publishing.
- Eynaud, F., Cronin, T.M., Smith, S.A., Zaragoza, S., Mavel, J., Mary, Y., Pujol, C., 2009. Morphological variability of the planktonic foraminifer *Neogloboquadrina pachyderma* from ACEX cores: Implications for Late Pleistocene circulation in the Arctic Ocean. *Micropaleontology* 101–116.
- Farmer, J.R., Sigman, D.M., Granger, J., Underwood, O.M., Fripiat, F., Cronin, T.M., Martínez-García, A., Haug, G.H., 2021. Arctic Ocean stratification set by sea level and freshwater inputs since the last ice age. *Nat. Geosci.* 14 (9), 684–689. <https://doi.org/10.1038/s41561-021-00789-y>.
- Goetz, E.J., Greco, M., Rappaport, H.B., Weiner, A.K.M., Walker, L.M., Bowser, S., Goldstein, S., Katz, L.A., 2022. Foraminifera as a model of the extensive variability in genome dynamics among eukaryotes. *BioEssays* 44 (10), 1–10. <https://doi.org/10.1002/bies.202100267>.
- Goldstein, S.T., 2002. 3. Foraminifera: a biological overview. In: Sen Gupta, B.K. (Ed.), *Modern Foraminifera*. Kluwer Academic Publishers, pp. 37–55.
- Gradinger, R., 1999. Integrated abundance and biomass of sympagic meiobfauna in Arctic and Antarctic pack ice. *Polar Biol.* 22 (3), 169–177. <https://doi.org/10.1007/s003000050407>.
- Greco, M., Jonkers, L., Kretschmer, K., Bijma, J., Kucera, M., 2019. Depth habitat of the planktonic foraminifera *Neogloboquadrina pachyderma* in the northern high latitudes explained by sea-ice and chlorophyll concentrations. *Biogeosciences* 16 (17), 3425–3437. <https://doi.org/10.5194/bg-16-3425-2019>.
- Greco, M., Morard, R., Kucera, M., 2021a. Single-cell metabarcoding reveals biotic interactions of the Arctic calcifier *Neogloboquadrina pachyderma* with the eukaryotic pelagic community. *J. Plankton Res.* 43 (2), 113–125. <https://doi.org/10.1093/plankt/fbab015>.
- Greco, M., Werner, K., Zamelczyk, K., Rasmussen, T.L., Kucera, M., 2021b. Decadal trend of plankton community change and habitat shoaling in the Arctic gateway recorded by planktonic foraminifera. *Glob. Change Biol.* 28 (5), 1798–1808. <https://doi.org/10.1111/geb.16037>.
- Grell, K.G., 1954. Der Generationswechsel der polythalamen Foraminifere *Rota~iella heterocaryotica*. *Arch. Protistenkd.* 100, 268–286.
- Hallock, P., Larsen, A.R., 1979. Cooling direction in amphistegina. *Marine Micropaleontol.* 4, 33–44. [https://doi.org/10.1016/0377-8398\(79\)90004-5](https://doi.org/10.1016/0377-8398(79)90004-5).

- Hallock, P., Reymond, C.E., 2022. Contributions of trimorphic life cycles to dispersal and evolutionary trends in large benthic foraminifers. *J. Earth Sci.* 33 (6), 1425–1433.
- Harney, J.N., Hallock, P., Talge, H.K., 1998. Observations on a Trimorphic Life Cycle in *Amphistegina gibbosa* Populations from the Florida Keys. *J. Foraminifer. Res.* 28 (2), 141–147. <https://doi.org/10.2113/gsj.Foraminifer.Res.28.2.141>.
- Hemleben, C., Spindler, M., Anderson, O.R., 1989. In: *Modern planktonic Foraminifera*. Springer, Berlin.
- Hillaire-Marcel, C., De Vernal, A., Polyak, L., Darby, D., 2004. Size-dependent isotopic composition of planktic foraminifers from Chukchi Sea vs. NW Atlantic sediments—implications for the Holocene paleoceanography of the western Arctic. *Quat. Sci. Rev.* 23 (3–4), 245–260.
- Holzmann, M., Pawłowski, J., 1996. Preservation of Foraminifera for DNA extraction and PCR amplification. *J. Foraminifer. Res.* 26 (3), 264–267. <https://doi.org/10.2113/gsj.Foraminifer.Res.26.3.264>.
- Hsiang, A.Y., Nelson, K., Elder, L.E., Sibert, E.C., Kahanamoku, S.S., Burke, J.E., Kelly, A., Liu, Y., Hull, P.M., 2018. AutoMorph: Accelerating morphometrics with automated 2D and 3D image processing and shape extraction. *Methods Ecol. Evol.* 9 (3), 605–612. <https://doi.org/10.1111/2041-210X.12915>.
- Huber, R., Meggers, H., Baumann, K.-H., Raymo, M.E., Henrich, R., 2000. Shell size variation of the planktonic foraminifer Neogloboquadrina pachyderma sin. in the Norwegian–Greenland Sea during the last 1.3 Myrs: Implications for paleoceanographic reconstructions. *Palaeogeogr. Palaeoclimatol. Palaeoecol.* 160 (3–4), 193–212. [https://doi.org/10.1016/S0031-0182\(00\)00066-3](https://doi.org/10.1016/S0031-0182(00)00066-3).
- Ingvaldsen, R.B., Assmann, K.M., Primicerio, R., Fossheim, M., Polyakov, I.V., Dolgov, A.V., 2021. Physical manifestations and ecological implications of Arctic Atlantification. *Nat. Rev. Earth Environ.* 2 (12), 874–889. <https://doi.org/10.1038/s43017-021-00228-x>.
- Kimoto, T., Tsuchiya, M., 2006. The “unusual” reproduction of planktic foraminifera: an asexual reproductive phase of *Neogloboquadrina pachyderma* (Ehrenberg). *Anuário do Instituto de Geociências UFRJ* 29, 461.
- Knudsen, K.L., Stabell, B., Seidenkrantz, M.-S., Eirksson, J., Blake Jr., W., 2008. Deglacial and Holocene conditions in northernmost Baffin Bay: Sediments, foraminifera, diatoms and stable isotopes. *Boreas* 37 (3), 346–376. <https://doi.org/10.1111/j.1502-3885.2008.00035.x>.
- Knyazeva, O., Korsun, S., 2016. High Arctic benthic foraminiferans during the polar night: Dormancy or active feeding? *Protistology* 10 (2). Article 2.
- Ko, E., Park, J., Cho, K.-H., Yoo, J., Moon, J.K., Shim, C., Yang, E.J., 2024. Revealing the seasonal cycles of Arctic phytoplankton: Insights from year-round chlorophyll monitoring. *Environ. Res. Lett.* 19 (2), 024028. <https://doi.org/10.1088/1748-9326/ad1c7e>.
- Kohfeld, K.E., Fairbanks, R.G., Smith, S.L., Walsh, I.D., 1996. Neogloboquadrina pachyderma (sinistral coiling) as paleoceanographic tracers in polar oceans: evidence from northeast water polynya plankton tows, sediment traps, and surface sediments. *Paleoceanography* 11 (6), 679–699. <https://doi.org/10.1029/96PA02617>.
- Krembs, C., Eicken, H., Junge, K., Deming, J.W., 2002. High concentrations of exopolymeric substances in Arctic winter sea ice: Implications for the polar ocean carbon cycle and cryoprotection of diatoms. *Deep-Sea Res. I Oceanogr. Res. Pap.* 49 (12), 2163–2181. [https://doi.org/10.1016/S0967-0637\(02\)00122-X](https://doi.org/10.1016/S0967-0637(02)00122-X).
- Le Calvez, J., 1946. Place de la reduction chromatique et alternance de phases nucleaires dans le cycle des foraminifères. *C. R. Hebd. Séances Acad. Sci.* 222, 612–614.
- Le Calvez, J., 1950. Recherches sur les Foraminifères. II. Place de la meiose et sexualité. *Arch. Zool. Exp. Gen.* 87, 211–244.
- Lebreton, R., Iovleff, S., Langrognet, F., Biernacki, C., Celeux, G., Govaert, G., 2015. Rmixmod: the R package of the model-based unsupervised, supervised, and semi-supervised classification Mixmod library. *J. Stat. Softw.* 67 (6), 1–29. <https://doi.org/10.18637/jss.v067.i06>.
- Leutenegger, S., 1977. Reproduction cycles of larger foraminifera and depth distribution of generations. In: Reiss, Z., Leutenegger, S., Hottinger, L., Fermont, W.J.J., Meulenkamp, J.E., Thomas, E., Hansen, H.J., Buchardt, B., Larsen, A.R., Drooger, C.W. (Eds.), *Depth-Relations of Recent Larger Foraminifera in the Gulf of Aqaba-Elat, 15. Utrecht Micropaleontological Bulletins*, pp. 27–34.
- Meiland, J., Ezat, M.M., Westgård, A., Manno, C., Morard, R., Siccha, M., Kucera, M., 2022. Rare but persistent asexual reproduction explains the success of planktonic foraminifera in polar oceans. *J. Plankton Res.* 45, 15–32. <https://doi.org/10.1093/plankt/fbac069>.
- Meiland, J., Siccha, M., Morard, R., Kucera, M., 2024. Continuous reproduction of planktonic foraminifera in laboratory culture. *J. Eukaryot. Microbiol.* 71 (3). <https://doi.org/10.1111/jeu.13022>.
- Morard, R., Darling, K.F., Weiner, A.K.M., Hassenrück, C., Vanni, C., Cordier, T., Henry, N., Greco, M., Vollmar, N.M., Milivojevic, T., Rahman, S.N., Siccha, M., Meiland, J., Jonkers, L., Quillévér, F., Escarguel, G., Douady, C.J., de Garidel-Thoron, T., de Vargas, C., Kucera, M., 2024. The global genetic diversity of planktonic foraminifera reveals the structure of cryptic speciation in plankton. *Biol. Rev.* 99 (4), 1218–1241. <https://doi.org/10.1111/brv.13065>.
- Myers, E.H., 1942. A quantitative study of the productivity of the foraminifera in the sea. *Proc. Am. Philos. Soc.* 325–342.
- Nicolaus, M., Petrich, C., Hudson, S.R., Granskog, M.A., 2013. Variability of light transmission through Arctic land-fast sea ice during spring. *Cryosphere* 7 (3), 977–986. <https://doi.org/10.5194/tc-7-977-2013>.
- Nørgaard-Pedersen, N., Mikkelsen, N., Lassen, S.J., Kristoffersen, Y., Sheldon, E., 2007. Reduced Sea ice concentrations in the Arctic Ocean during the last interglacial period revealed by sediment cores off northern Greenland. *Paleoceanography* 22 (1). <https://doi.org/10.1029/2006PA001283>.
- Ofstad, S., Zamelczyk, K., Kimoto, K., Chierici, M., Fransson, A., Rasmussen, T.L., 2021. Shell density of planktonic foraminifera and pteropod species *Limacina helicina* in the Barents Sea: Relation to ontogeny and water chemistry. *Plos One* 16 (4), e0249178. <https://doi.org/10.1371/journal.pone.0249178>.
- Parker, A.H., Wilkinson, S.W., Ton, J., 2022. Epigenetics: a Catalyst of Plant Immunity against Pathogens. *New Phytol.* 233 (1), 66–83. <https://doi.org/10.1111/nph.17699>.
- Perovich, D.K., 2007. Light reflection and transmission by a temperate snow cover. *J. Glaciol.* 53 (181), 201–210. <https://doi.org/10.3189/172756507782202919>.
- Perovich, D.K., 2017. Chapter 4 Sea ice and sunlight. In: Thomas, D.N. (Ed.), *Sea Ice* Third Edition. Wiley Blackwell, pp. 110–137. <https://doi.org/10.1002/9781118778371>.
- Pflaumann, U., Duprat, J., Pujol, C., Labeyrie, L.D., 1996. SIMMAX: a modern analog technique to deduce Atlantic Sea surface temperatures from planktonic foraminifera in deep-sea sediments. *Paleoceanography* 11 (1), 15–35. <https://doi.org/10.1029/95PA01743>.
- Polyakov, I.V., Pnyushkov, A.V., Alkire, M.B., Ashik, I.M., Baumann, T.M., Carmack, E.C., Goscicko, I., Guthrie, J., Ivanov, V.V., Kanzow, T., Krishfield, R., Kwok, R., Sundfjord, A., Morison, J., Rembert, R., Yulin, A., 2017. Greater role for Atlantic inflows on sea-ice loss in the Eurasian Basin of the Arctic Ocean. *Science* 356 (6335), 285–291. <https://doi.org/10.1126/science.aai8204>.
- Prabhakar, M., Thirumalai, K., Cronin, T.M., Gemery, L., Thomas, E.K., Rafter, P.A., 2024. Morphotypical and geochemical variations of planktic foraminiferal species in Siberian and central Arctic ocean core tops. *J. Foraminiferal Res.* 54 (1), 1–19.
- RStudio Team, 2020. RStudio: Integrated Development for R. RStudio, PBC, Boston, MA. URL: <http://www.rstudio.com/>.
- Sautter, L.R., Thunell, R.C., 1989. Seasonal succession of planktonic foraminifera; results from a four-year time-series sediment trap experiment in the Northeast Pacific. *J. Foraminif. Res.* 19 (4), 253–267. <https://doi.org/10.2113/gsjfr.19.4.253>.
- Schiebel, R., Spilhagen, R.F., Garnier, J., Hagemann, J., Howa, H., Jentzen, A., Martínez-García, A., Meilland, J., Michel, E., Repschläger, J., Salter, I., Yamasaki, M., Haug, G., 2017. Modern planktic foraminifers in the high-latitude ocean. *Marine Micropaleontol.* 136, 1–13. <https://doi.org/10.1016/j.marmicro.2017.08.004>.
- Schneider, C.A., Rasband, W.S., Eliceiri, K.W., 2012. NIH image to ImageJ: 25 years of image analysis. *Nat. Methods* 9 (7), 671–675. <https://doi.org/10.1038/nmeth.2089>.
- Siccha, M., Kucera, M., 2017. ForCenS, a curated database of planktonic foraminifera census counts in marine surface sediment samples. *Sci. Data* 4 (1), 170109. <https://doi.org/10.1038/sdata.2017.109>.
- Sigler, M.F., Stabeno, P.J., Eisner, L.B., Napp, J.M., Mueter, F.J., 2014. Spring and fall phytoplankton blooms in a productive subarctic ecosystem, the eastern Bering Sea, during 1995–2011. *Deep-Sea Res. II Top. Stud. Oceanogr.* 109, 71–83. <https://doi.org/10.1016/j.dsrr.2013.12.007>.
- Snoeijis-Leijonmalm, P., the SAS-Oden Scientific Party, 2022. *Expedition Report SWEDARCTIC Synoptic Arctic Survey 2021 with icebreaker Oden*. Swedish Polar Research Secretariat, pp. 1–310.
- Spindler, M., Dieckmann, G.S., 1986. Distribution and abundance of the planktic foraminifer Neogloboquadrina pachyderma in sea ice of the Weddell Sea (Antarctica). *Polar Biol.* 5 (3), 185–191. <https://doi.org/10.1007/BF00441699>.
- Takagi, H., Kurasawa, A., Kimoto, K., 2020. Observation of asexual reproduction with symbiont transmission in planktonic foraminifera. *J. Plankton Res.* 42 (4), 403–410. <https://doi.org/10.1093/plankt/fbaa033>.
- Thompson, P.R., Shackleton, N.J., 1980. North Pacific palaeoceanography: late Quaternary coiling variations of planktonic foraminifer Neogloboquadrina pachyderma. *Nature* 287 (5785), 829–833. <https://doi.org/10.1038/287829a0>.
- Vermassen, F., Bird, C., Weitkamp, T.M., Darling, K.F., Farnelid, H., Heuzé, C., Hsiang, A.Y., Karam Stranne, C., Sundbom, M., Coxall, H.K., 2025. The distribution and abundance of planktonic foraminifera under summer sea ice in the Arctic Ocean. *Biogeosciences* 22 (9), 2261–2286. <https://doi.org/10.5194/bg-22-2261-2025>.
- Vilks, J., 1973. *A Study of Globorotalia Pachyderma (Ehrenberg) =Globigerina pachyderma (Ehrenberg) in the Canadian Arctic*. PhD Dissertation. Department of Oceanography, Dalhousie University, Halifax, Nova Scotia.
- Vilks, G., 1975. Comparison of Globorotalia pachyderma (Ehrenberg) in the water column and sediments of the Canadian Arctic. *The Journal of Foraminiferal Research* 5 (4), 313–325. <https://doi.org/10.2113/gsjfr.5.4.313>.
- Vilks, G., 1989. Ecology of recent Foraminifera on the Canadian Continental Shelf of the Arctic Ocean. In: Herman, Y. (Ed.), *The Arctic Seas*. Springer US, pp. 497–569. https://doi.org/10.1007/978-1-4613-0677-1_21.
- Weiner, A.K.M., Cerón-Romero, M.A., Yan, Y., et al., 2020. Phylogenomics of the Epigenetic Toolkit reveals Punctate Retention of Genes across Eukaryotes. *Genome Biol. Evol.* 12 (12), 2196–2210. <https://doi.org/10.1093/gbe/eva198>.
- Xiao, W., Wang, R., Polyak, L., Astakhov, A., Cheng, X., 2014. Stable oxygen and carbon isotopes in planktonic foraminifera *Neogloboquadrina pachyderma* in the Arctic Ocean: an overview of published and new surface-sediment data. *Mar. Geol.* 352, 397–408. <https://doi.org/10.1016/j.margeo.2014.03.024>.
- Zamelczyk, K., Fransson, A., Chierici, M., Jones, E., Meiland, J., Anglada-Ortiz, G., Lødemel, H.H., 2021. Distribution and Abundances of Planktic Foraminifera and Shelled Pteropods during the Polar Night in the Sea-Ice Covered Northern Barents Sea. *Front. Mar. Sci.* 8 (644094), 1–19. <https://doi.org/10.3389/fmars.2021.644094>.